Electrochimica Acta 544 (2025) 147563

Contents lists available at ScienceDirect

Electrochimica Acta

journal homepage: www.journals.elsevier.com/electrochimica-acta

Reevaluating mechano-driven chemical reactions: Insights from ultrasonic, piezo, and contact-electro mechanisms

Sidra Tul Muntaha [a,b], Zhong Lin Wang [a], Di Wei [a,*]

[a] Beijing Institute of Nanoenergy and Nanosystems, Chinese Academy of Sciences, Beijing 101400, People's Republic of China
[b] School of Nanoscience and Engineering, University of Chinese Academy of Sciences, Beijing 100049, People's Republic of China

ARTICLE INFO

Keywords:
Ultrasound
Contact electrification
Sonocatalysis
Piezocatalysis
Contact-electro catalysis
Photocatalysis

ABSTRACT

Mechano-driven chemical reactions offer a disruptive alternative to conventional thermally and photochemically initiated processes. However, conceptual ambiguities, particularly conflating sonochemistry with piezocatalysis, have obscured a coherent understanding of these mechanistic pathways. This review reexamines mechano-activation through a unified energy-transfer perspective, focusing on three representative mechanisms: sonochemistry, piezocatalysis, and contact-electro catalysis (CEC). We dissect how ultrasonic excitation spans a frequency- and intensity-dependent continuum, from low-frequency ultrasound (20–100 kHz) that enhances mass transport and interfacial effects, to high-frequency ultrasound (>100 kHz) capable of inducing bond cleavage via transient high-temperature and high-pressure microenvironments generated by acoustic cavitation. In contrast, piezocatalysis and CEC rely on mechanical-to-electrical transduction mechanisms via piezoelectric polarization or interfacial charge transfer, respectively, offering photonic- and adsorption-independent activation pathways with high catalyst recyclability. By re-evaluating the driving forces and energetic thresholds underlying each mechano-chemical pathway, this review clarifies the mechanistic boundaries and operational regimes of ultrasonics, piezoelectric, and contact-electro-induced reactions. Emphasis is placed on the critical role of material properties and the importance of decoupling mechanical and electronic descriptors. The review concludes by outlining key directions for the rational design of mechano-responsive materials and catalytic systems, offering new opportunities for sustainable catalysis and next-generation mechano-driven chemical reactions.

1. Introduction

Mechanochemistry, where chemical transformations are driven by mechanical force such as grinding, shear, or milling, offers a solvent-free, energy-efficient alternative to conventional thermal or photochemical methods [1]. Though historically rooted in ancient practices like cinnabar grinding, systematic study emerged in the 19th century through the pioneering work of Michael Faraday and Matthew Carey Lea [2,3]. Wilhelm Ostwald formally defined mechanochemistry as a distinct field in 1919, yet its broader adoption only accelerated in recent decades with advancements in analytical tools and mechanochemical equipment [4]. Among the most promising developments is the integration of ultrasound as a mechanical energy source.

Modern ultrasonic technologies trace their origin to the discovery of the piezoelectric effect by Jacques and Pierre Curie in 1880. This principle, where mechanical stress generates electric polarization in specific crystals, underpins ultrasonic transducers, which convert alternating voltages into high-frequency mechanical vibrations. These vibrations, particularly in liquids, generate acoustic cavitation: the formation, growth, and violent collapse of microbubbles. This phenomenon produces transient localized conditions of extreme temperature and pressure, making ultrasound a powerful driver of both physical transformations and chemical reactions [5].

Cavitation is a complex, nucleation-dependent process influenced by acoustic frequency, intensity, and reactor design. It manifests in two forms: transient cavitation, which drives high-energy reactions through violent collapse, and stable cavitation, which contributes through sustained oscillations and microstreaming. The prevailing "hot spot" model suggests that each collapse creates a microreactor with temperatures exceeding 4500 K and pressures above 1000 atm, conditions capable of initiating bond cleavage and radical formation. These localized effects underpin sonochemistry, a field formally recognized in the late 1980s,

* Corresponding author.
E-mail addresses: sidratulmuntaha@binn.cas.cn (S.T. Muntaha), zlwang@binn.cas.cn (Z.L. Wang), weidi@binn.cas.cn (D. Wei).

https://doi.org/10.1016/j.electacta.2025.147563
Received 4 August 2025; Received in revised form 1 October 2025; Accepted 11 October 2025
Available online 13 October 2025

and now widely applied in synthesis, degradation, and catalysis [6].

In heterogeneous systems, the collapse of bubbles near solid surfaces introduces additional mechanical phenomena, such as microjets, surface erosion, and particle collisions that enhance mass and heat transfer, particle dispersion, and catalytic surface activation. These physical effects form the basis of sonocatalysis, where ultrasound accelerates chemical transformations via interfacial or particulate mechanisms [7]. Despite its broad applicability, the mechanistic underpinnings of sonocatalysis are often conflated with those of piezocatalysis, in which mechanical deformation of piezoelectric materials induces charge separation and drives redox reactions independently of cavitation or light [8].

Furthermore, recent developments in contact-electro-catalysis (CEC), a mechano-driven process where interfacial charge transfer is activated via solid–liquid contact electrification, have introduced an entirely new platform for energy-independent catalysis. Unlike piezocatalysis, which relies on bulk polarization, CEC exploits triboelectric effects at material interfaces, allowing for redox chemistry without external voltage, light, or noble metals [9].

Although the literature contains several comprehensive reviews on sonochemistry, piezocatalysis, and CEC as separate topics [6,9,10]. The rapid expansion of piezocatalysis research in recent years has blurred the mechanistic boundaries among these fields. With the growing popularity of piezocatalysis, an increasingly wide range of materials, regardless of whether they possess non-centrosymmetric structures, have been examined under this framework [11]. Moreover, many emerging materials exhibit hybrid characteristics that span multiple mechanistic regimes, yet their catalytic behavior is often interpreted exclusively through the lens of a single research tradition. This practice overlooks potential synergistic effects and obscures the interdependence of underlying mechanisms, thereby reinforcing conceptual ambiguity rather than resolving it [12–14] (Fig. 1).

This review reexamines mechano-driven chemical reactions through a comparative lens, by focusing on ultrasound as a tunable mechanical driver, we categorize activation mechanisms across frequency and intensity regimes, distinguishing mechanical from chemical contributions. We emphasize the importance of cavitation control for desired outcomes and discuss how piezoelectric and triboelectric materials convert mechanical inputs into catalytic function. The primary objective of our work is to provide the first systematic comparative analysis of three emerging yet mechanistically intertwined fields: sonocatalysis, piezocatalysis, and the newly developing concept of contact-electro-catalysis.

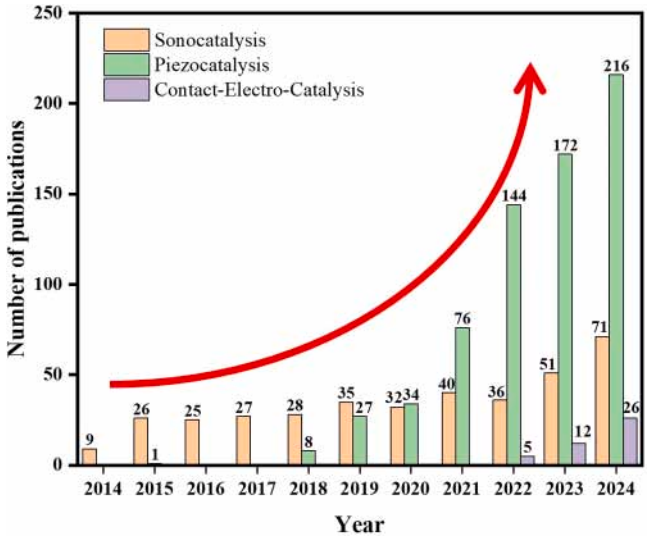

Fig. 1. Number of publications on sonocatalysis, piezocatalysis and CEC. The data is extracted from web of science using the keywords Sonocatalysis, Piezocatalysis and Contact Eletro Catalysis.

To date, the boundaries between these mechano-driven catalytic processes remain indistinct in the literature, creating substantial challenges for mechanistic interpretation and theoretical advancement. By organizing these mechanisms side by side, we aim to lay the groundwork for future development of a quantitative or unified energy-transfer theory, which the current body of literature is not yet mature enough to support.

2. Ultrasound and sonochemistry

2.1. Ultrasonic parameters

Pressure waves, which are cycles of compression and expansion, travel through a gas, liquid, or solid to produce sound. Newton, who was interested in sound propagation, was likely the first person to explain the connections between the speed of sound and measurable features of the medium, such as density and pressure, in his 1687 Principia [15,16]. Humans can detect these pressure waves if the frequencies fall between 10 Hz and roughly 18 kHz (the Hertz unit denoting one cycle of compression or rarefaction per second). Hence, ultrasound has frequencies beyond human hearing, above 20 kHz [17]. These frequencies above 20 kHz are further divided and are being used for different purposes. The frequency range between 20 kHz to 100 kHz is the range of conventional power ultrasound. The extended range goes to 1 MHz. The frequencies from 1 MHz to 10 MHz are increasingly being used for diagnostics (Fig. 2) [18]. The frequencies below human hearing can be called infrasound [19].

Conventional power ultrasound (20 kHz–1 MHz) gained increasing attention in the late 19th century due to its frequency- and amplitude-dependent physical and chemical effects [6]. These tunable parameters have enabled its widespread application across diverse fields based on specific frequency and power requirements. For example; diagnostic ultrasound is employed in medicine (echography) for fetal and soft-tissue imaging because they have much shorter wavelengths and, therefore, better resolution in detecting phase changes [21]. Ultrasound irradiation is considered safe and the preferred diagnostic option during early pregnancy, provided that the acoustic intensity remains within recommended low levels [22]. Several parameters, including frequency and power, determine whether ultrasound influences the chemical reaction pathway or solely its physical effects. These parameters have been discussed in detail by Wood et al. in their parametric review of sonochemistry [23]. They divided all parameters into two main categories. Primary parameters include amplitude, frequency, and reactor design. While secondary parameters include solid addition, surfactants, changes in liquid properties, and the effect of gases (Fig. 3). For a given reactor design, amplitude and frequency remain the most critical and readily tunable parameters. These variables can selectively trigger chemical pathways or exploit purely physical effects of ultrasound.

2.2. Sonochemistry: ultrasound-induced chemical transformations

The earliest reports on chemical effects driven by high-frequency ultrasound (100–500 kHz) dated back to the late 1920s [26]. Frequency effects were primarily responsible for the observed speed of some chemical reactions. Then, in 1979, a paper revealing the true sonochemical effect appeared. It explained that when the aqueous solution with dissolved oxygen is irradiated, it produces hydrogen peroxide (H_2O_2) at frequencies 750 kHz and 250 W power [27].

Sonochemistry was explored in aqueous solution for over a decade, as the sound waves of high frequency pass through the aqueous solution; they generate negative pressure in the medium, which then results in the formation, growth, and eventual collapse of the bubble, this is the process which is being called cavitation collapse. Although it is difficult to find a theory that can explain the nature of cavitation, a model known as the "hot spot" is supported by a large body of experimental data shown in Fig. 4a. This indicates that a temporary, localised entity (hot spot) with temperatures will be rapidly quenched by the surrounding liquid

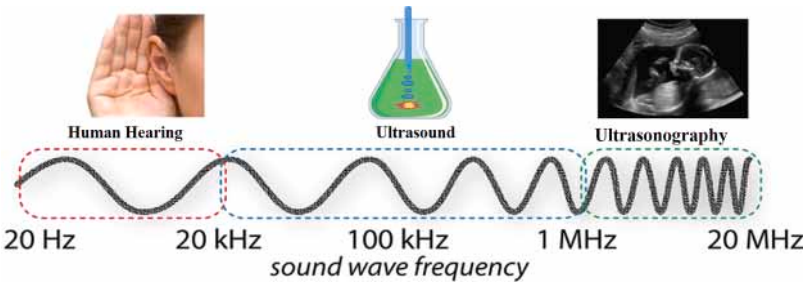

Fig. 2. Sound wave spectrum with the regions of interest, reproduced with permission from McKenzie et al. [20] Copyright 2019, John Wiley and Sons.

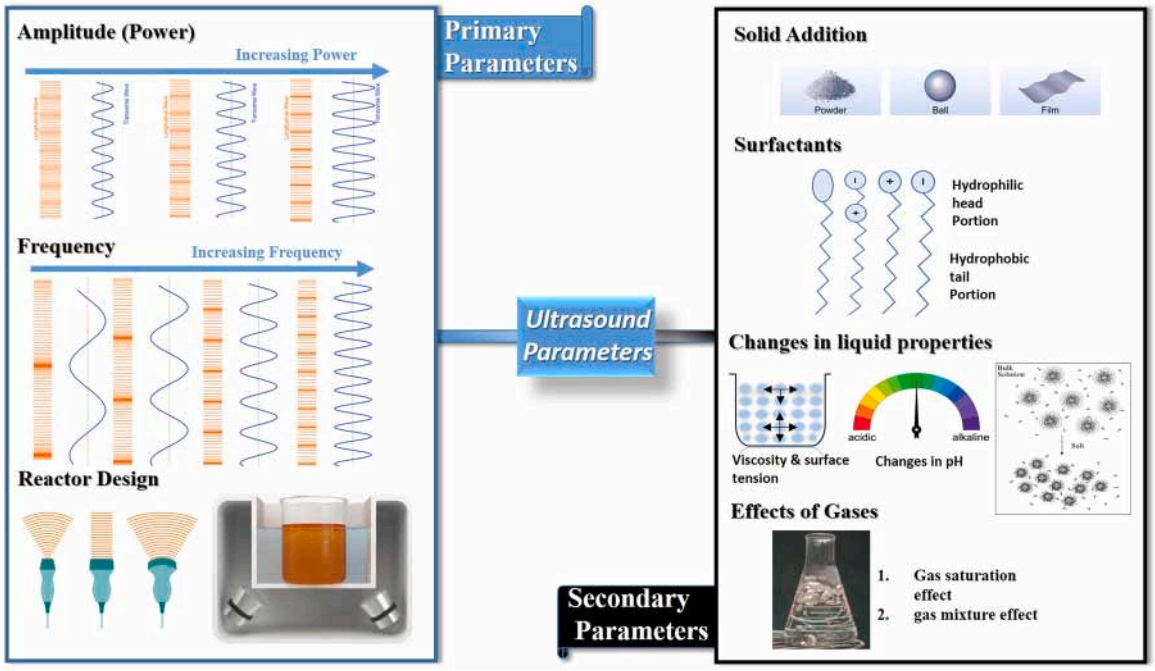

Fig. 3. Different categories of parameters that can influence the chemistry in ultrasound. Reproduced with permission from the reference [24,25] copyright 2022, Springer Nature & 2024, Elsevier.

following cavity collapse. Between 4500 and 5000 K and pressures greater than 1000 atmospheres. With a lifetime of only a few microseconds and cooling rates of roughly 1010 K^{-1}, this quasi-adiabatic high-energy process significantly affects the cavitating liquid's physical characteristics and determines the chemical destiny of volatile species in particular [27–30].

Frequency and Power of the ultrasound both play a dominant role in sonochemistry. The enhancement of sonochemical effects with increasing power has been extensively documented in the literature. According to Sehgal and Wang [31], thymine decomposition in aqueous solutions increased over the intensity range of 0.5–3 W/cm^2 at 990 kHz (measured as a percentage change in thymine concentration). In the power range of 0.3–2 W/cm^2 at 1 MHz frequency, Gutierrez and Henglein [32] have noted an increase in the rate of iodide oxidation in tandem with an increase in acoustic power levels. They stated that a maximum rate for the sonochemical oxidation of iodide was observed at an optimal power intensity of 2 W/cm^2. Henglein et al. [33] irradiated luminol and iodide solutions with 800 kHz ultrasonic pulse trains, the corresponding luminescence trains were examined, and the iodide yields were calculated. The chemical yield and luminescence rise with increasing sound intensity in continuous irradiation up to roughly 2.5 W/cm^2, but they quickly fall at higher intensities Fig. 4b. Kanthale et al. [34] measured the H_2O_2 yield at different irradiation frequencies and intensities. The trend for the yield of H_2O_2 increased with the increasing intensity, along with an increase in frequency, as shown in the Fig. 4e but the trend somewhat showed the optimal threshold for the frequency; the maximum yield was observed at the frequency of 355 kHz, with the further increase in frequency, the yield decreased. Christian Petrier [35] and his colleagues discussed the unexpected frequency effects on the rate of oxidative process, and they compared a high frequency of 514 kHz with the more commonly used 20 kHz frequency and described that under extreme frequency conditions of 514 kHz, the yields of hydrogen and hydroxyl radicals (·OH) were higher as compared with the low frequency. The extreme difference can be seen in the Fig. 4c. Muthupandian Ashokkumar and his colleagues [36] measured the production of ·OH radicals generation at different frequencies and reported that the optimal generation of hydroxyl radicals can be found at 358 kHz Fig. 4f.

There has been widespread observation of an increase in the quantity of reactive species with the increase in frequency [39–41]. It is now well established that ultrasonic irradiation of aqueous solutions leads to varying rates of ·OH radical formation. Due to cavitation inefficiencies, radical formation rates are reduced at both low (~20 kHz) and very high (>1 MHz) ultrasonic frequencies, with optimal yields typically observed within the 300–800 kHz range [36]. Furthermore, at various operating frequencies, there are notable differences in the bubble size and size distribution as can be seen in Fig. 4(g) [38]. This is attributed to the presence of a threshold intensity in most systems, below which the supplied energy is insufficient to initiate cavitation. The intensity or

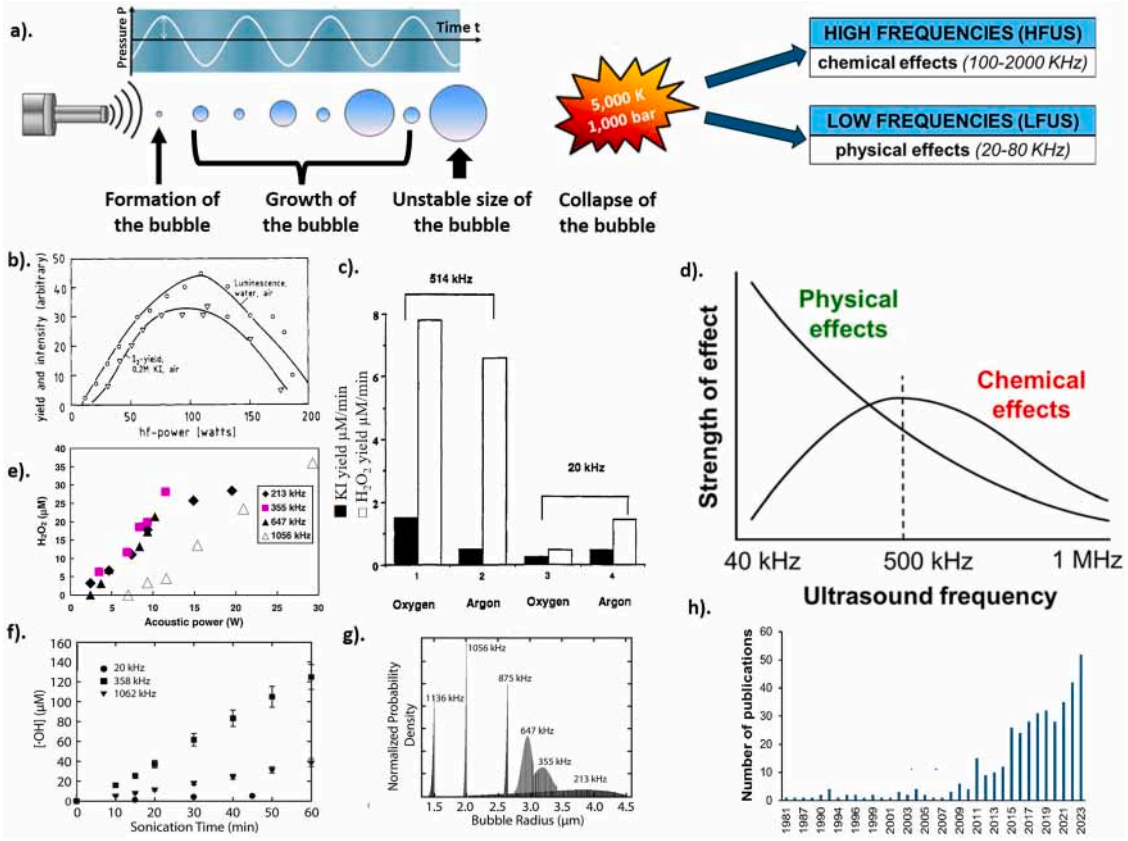

Fig. 4. a). Sonochemical activity, reproduced with permission from Chatel et al. [37] Copyright 2016, Elsevier. b). Yield and luminescence intensity of iodine as a function of acoustic power reproduced with the permission of Henglein et al. [33] Copyright American chemical Society (ACS), 1989 c). Comparative formation rates for hydrogen peroxide (□) in water at 514 and 20 kHz, as well as triiodide in KI and 10^{-2} M solution (■) for solutions saturated with oxygen or argon, reproduced with permission from Petrier et al. [35] Copyright ACS, 1992 d). Contribution of physical and chemical effects of ultrasound at different frequencies produced from shear forces and reactive radicals, reproduced with permission from McKenzie et al. [20] Copyright 2019, John Wiley and Sons. e). Production of H_2O_2 at different frequencies and intensities. Adapted from reference [34] copyright ACS, 2008. f). Rate of hydroxyl radical generation at different frequencies as a function of time. g). Radius of bubbles at different frequencies. Figures e and f are adapted from references [36,38] with permission. Copyright 2008, Elsevier and the American Physical Society (ACS), 2009. h). Number of publications in which the word "sonocatalysis" appeared, from Scopus search, September 2024, reproduced with permissions from Trinh et al. [6] copyright The Royal Society of Chemistry (RCS), 2024.

power thus governs whether cavitation occurs, making it a critical parameter to consider in tailoring reaction outcomes. Ultrasound can cause cavitation events in any liquid as long as the right frequency and power are used [17]. This makes it possible for ultrasound to have a wide range of applications, whether it be in sonochemistry [6] or in mechano-driven chemical reactions [1].

2.3. Physical effects from ultrasound

The operating conditions of the process determine whether the physical or the chemical effects of ultrasound predominate. The applied frequency of the ultrasound is the most crucial factor. Physical effects predominate at lower frequencies (<100 kHz), whereas radical formation is frequently insignificant (Fig. 4a). These procedures are referred to as low-frequency ultrasound (LFUS). The physical effects of cavitation,

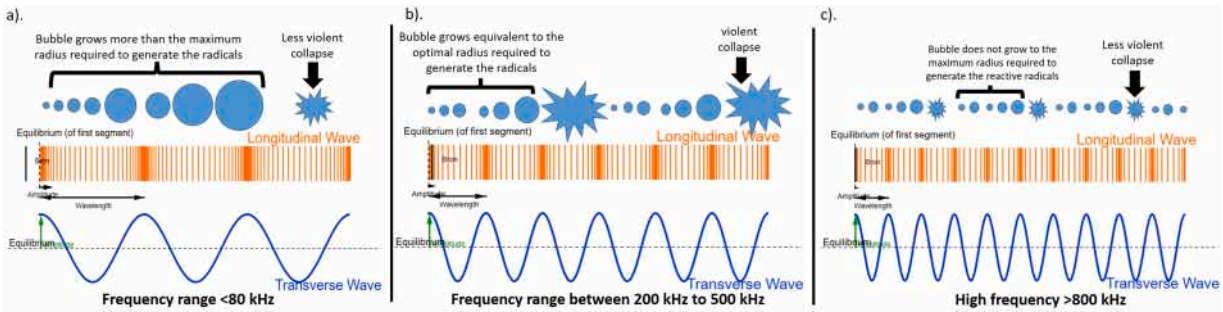

Fig. 5. Different frequency ranges and their effects at constant power. a) Low-frequency ultrasound; bubbles grow more than the maximum radius for the generation of radicals; therefore, chemical effects are negligible while physical effects dominate. b) Optimal frequency range for radical generation, i.e., bubble size is favorable to the required radius for the radical generation; therefore, chemical effects dominate. c) Bubble radius is less than the required minimum radius for the generation of reactive radicals created using GeoGebra.

including mixing, catalyst dispersion, and coke removal, are utilized in LFUS systems to increase reaction rates [36]. As a result, ultrasound, which operates between 200 and 500 kHz, is thought to be the ideal range for optimizing the chemical effects of ultrasound, which is usually referred to as high-frequency ultrasound (HFUS) (Fig. 5b).

The physical effects generated by collapsing cavitation bubbles can be harnessed to drive chemical transformations, enabling the successful synthesis of diverse organic and inorganic compounds and materials [42,43]. Furthermore, certain compounds or molecules can be activated to exert a mechanochemical response by dissolved species in the immediate vicinity of the collapsing bubble that are subjected to strong shear forces due to the microjets of liquid rushing to fill the bubble. Several classes of mechano-active catalysts have emerged as useful reagents for driving chemical transformations under the application of force, or mechanical energy [44]. Two of the well-known catalysts that utilize the physical effect of ultrasound to conduct mechano-driven reactions are Piezocatalysis and CEC, in which mechanical effects of ultrasound are harnessed to drive chemical reactions [1]. In these catalysis systems, the frequency of ultrasound remains less than or equivalent to 40 kHz [24].

3. Sonocatalysis and its fundamentals

It has been widely observed in literature that the addition of any solid/liquid in the aqueous medium, under ultrasound, has the ability to increase the yield/reactivity of the chemical process by a million-fold. This addition of solid/liquid that acts as a catalyst makes the whole process heterogeneous. Heterogeneous sonocatalysis, liquid-liquid or solid-liquid, has been largely utilized for wastewater treatment, [45,46] production of organic compounds, therapeutic processes, and biological applications since 2015 [6]. A wide range of catalysts has been employed as sonocatalysts, broadly classified into photo-thermal systems, [7,47,48] adsorbent-based systems, [49] and heterogeneous systems, such as metal-doped, zero-valent metal, [50] metal oxide, [51] and Sono-Fenton-like catalysts, [52] designed to exploit synergistic effects. In biological contexts, enzymatic and bioorthogonal catalytic systems have also been explored [53,54]. Each system operates via distinct underlying mechanisms.

A general fundamental mechanism of sonocatalysts can be described via Fig. 6. The ultrasound waves generate negative and positive pressure in the aqueous medium. The negative pressure regions create vacuum spaces in the aqueous media. These vacuum spaces grow equally in all directions as the negative pressure in the medium increases and are thus called bubbles. The presence of solid particles provides nucleation sites for these bubbles to grow. These nucleation sites disrupt the radial symmetry of the growing bubbles; thus, the growth of bubbles initiated by nucleation sites is asymmetric, and this asymmetric collapse leads to the formation of changes in the solid energy bands [5,55]. These asymmetric and frequent collapse near the solid surfaces provides enough energy to transfer electrons from the conduction band to the valence band. These electrons are being captured by H_2O_2 molecules present in the aqueous solution, which are formed by the symmetric cavitation collapses occurring in the homogeneous phase. The H_2O_2 molecules are reduced to reactive oxygen species (ROS) [56,57]. ROS takes part in the chemical reaction. Furthermore, many factors can significantly impact the bubble nucleation rate at the solid surface: (1) the sonication parameters (ultrasound frequency, solution temperature, surfactant presence [58], dissolved gas type [59], etc.) and (2) physicochemical characteristics (wettability [58,60], pore characteristics [61], roughness [62], and particle size [58]) of the solid particles.

One of the central aims of this review is on the influence of added solid materials on the reaction process, as well as the associated changes in their physicochemical properties upon incorporation. Sonocatalysis utilizes a broad range of frequencies, power ranges, and temperatures. For example: Pandit et al. [63] degraded 2, 4, 6 Trichlorophenol 100mgL^{-1} in the presence of TiO_2 at the frequency of 22.7 kHz and 600 W power. Adsorption, desorption, and oxidation all contributed to the overall disappearance of the pollutant. The bulk solution's oxidation also contributed to the disappearance and overall degradation was only up to 50 % [63]. Wang et al. (2005) utilized TiO_2 (0.5–0.75gL^{-1}) in order

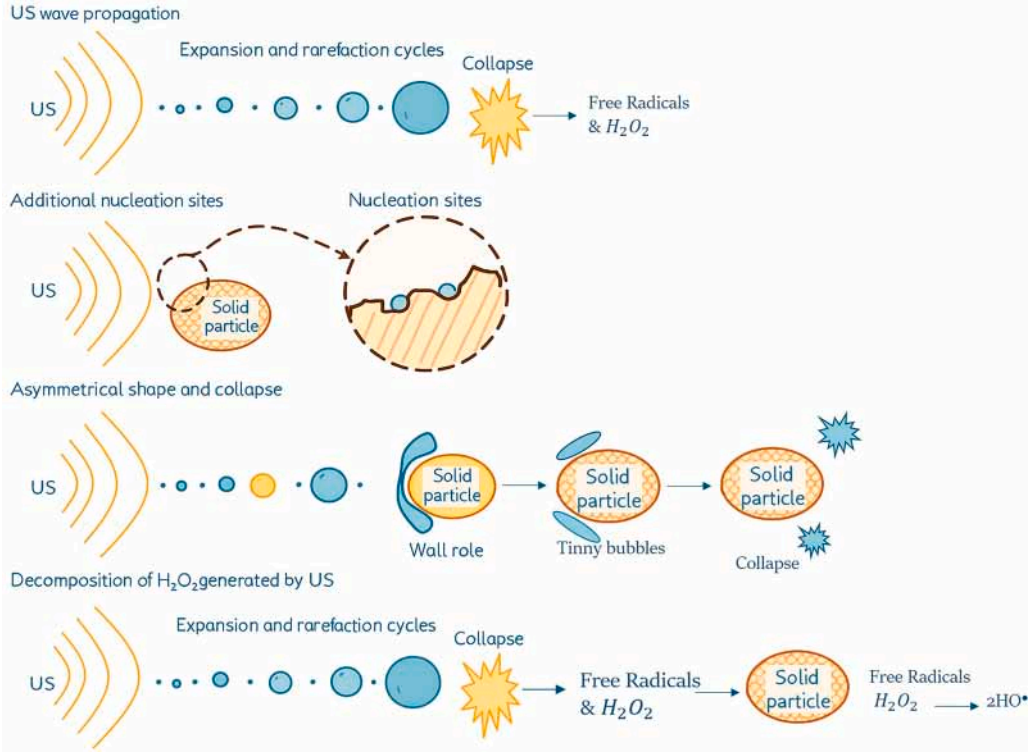

Fig. 6. a) A general fundamental principle of sonocatalyst systems. Reproduced with permission from the reference [5] copyright CRC Press (Taylor & Francis Group) 2012.

to degrade methyl orange (MO) (10–20mgL^{-1}) at 40–60 kHz frequency, 50 W/cm^2 power, while temperature was maintained at 40 °C [64]. Many such experiments utilizing a wide range of frequencies and power from 20 to 900 kHz and 50 to 600 W/cm^2 can be found in the literature at different temperatures exceeding up to 50 °C [65–68]. The reaction mechanism favored by ultrasound largely depends on the type of solid particles employed. Consequently, a variety of mechanisms have emerged over time. Several representative sonocatalytic mechanisms to be discussed in detail in this review are illustrated in Fig. 7. Nevertheless, the inclusion of solid particles introduces a substantial influence from surface chemistry in addition to improving nucleation sites. Because different materials have different surface functional groups and chemical properties, even under the same experimental conditions, the catalytic efficiency varies significantly.

3.1. Fundamental mechanism of photo-thermal-based catalytic systems

To effectively exploit the substantial sonoluminescence (SL) and thermal energy generated through acoustic cavitation, semiconductor photocatalysts, widely recognized as efficient sonocatalysts, simultaneously exhibit heterogeneous nucleation behavior and integrated photo-thermal-catalytic functionalities. A variety of semiconductor photocatalysts, including TiO_2, ZnO, BiOI, AgBr, $LuFeO_3$, and others, have been evaluated as sonocatalysts for the degradation of organic pollutants. The most extensively studied sonocatalyst is TiO_2 [13,69].

According to the photocatalytic mechanism, when cavitation bubbles collapse, SL is released with a broad wavelength range (200–700 nm) and a comparatively high intensity (0.098 W, or 400 nm) [70–73]. According to this viewpoint, a semiconductor material present in a cavitating ultrasonic system may be excited to form electron-hole pairs by light energy from SL greater than the semiconductor's band gap, further producing $\cdot O_2$ and ·OH at the conduction band (CB) and valence band (VB), respectively. This viewpoint is greatly inspired by the semiconductor photocatalytic mechanism [70–72]. According to the thermal catalytic mechanism, the semiconductor may be thermally excited by the high local temperature, which could also result in the creation of electron-hole pairs. High temperatures have been used to excite certain semiconductors (TiO_2, Cr_2O_3, etc.) in order to produce electron-hole pairs, according to numerous studies [74–77]. For instance, Mizuguchi et al. [76] discovered that when the mixture was heated to about 600 K, the full breakdown of polycarbonate (PCB) was accomplished in the presence of rutile TiO_2, whereas PCB by itself did not exhibit any decomposition. The sequential oxidation of PCB via the thermally excited positive holes on the TiO_2 surface was the cause of the high degradation performance. This mechanism is supported by several experiments that demonstrate that solid surfaces can be heated to 2700 K, which is significantly higher than this temperature, when ultrasonically generated bubbles collapse [78,79].

Since both photocatalytic and thermal catalytic mechanisms produce the same catalytic phenomenon, it is still unclear which mechanism dominates the overall sonocatalytic reaction rate. There are currently far more studies supporting the first viewpoint than the second. Nevertheless, there is currently no data that can be used to quantitatively settle the dispute. Since it is still unclear how much each of the two suggested mechanisms contributes, therefore, in literature, it is refer that the process of electron-hole pairs being formed on a semiconductor photocatalyst by heat and light as a photo-thermal-catalytic mechanism rather than talking about it separately. Since, it is still unclear whether it is heat or SL that causes the formation of holes and electrons, both theories collectively agree upon the transfer of electrons from VB to the CB, therefore, a general photo-thermal-catalytic process can be illustrated via Fig. 7(a). The photothermal sonocatalytic systems are limited in their ability for light absorption. The rapid recombination rate of generated holes and electrons is also a major factor in decreasing their efficiency. Along with this, they possess a low adsorption rate. Over time, various techniques to increase the sonocatalytic efficiency of photocatalytic semiconductors have evolved, such as doping with metal/co-metals and coupling with other semiconductors of a shorter bandgap [80–82]. Schematic illustrations of transition metal ions and noble metal-loaded sonocatalytic mechanisms (inspired from photocatalysis) are shown in Fig. 8a and 8b. Even though by the doping of various materials, the catalytic efficiency can be greatly enhanced. These various ways of doping and composite forming introduce critical trade-offs that require careful choice of material along with careful experimentation, which increases production cost [83,84].

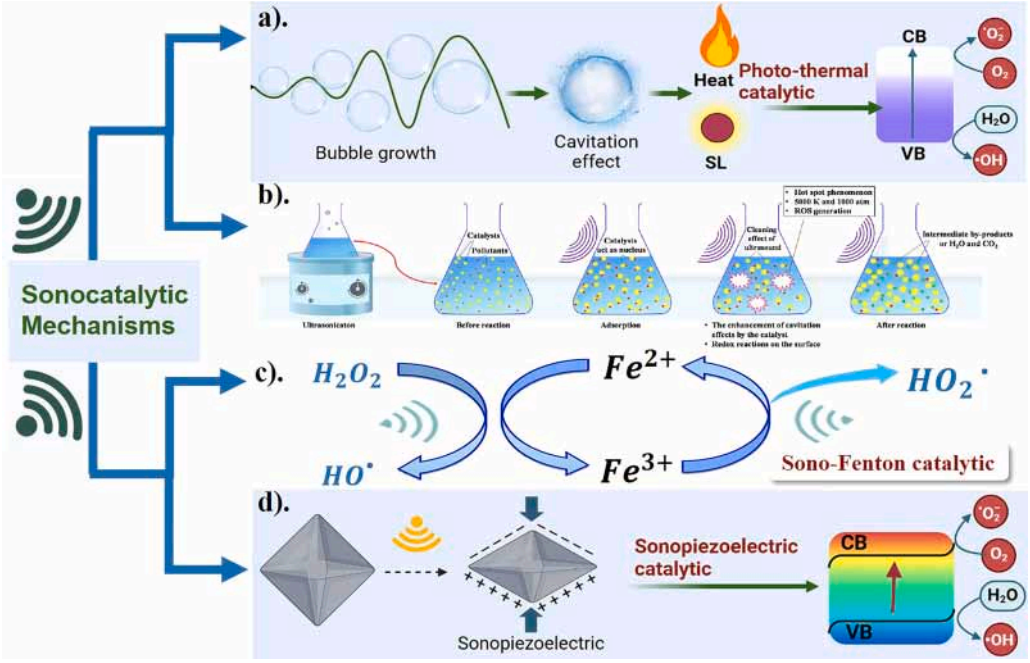

Fig. 7. Sonocatalysis Mechanisms: a). Photo-thermal sonocatalysis [54]. b) sonoadsorption [49]. Copyright Elsevier, 2019 c). Sonofenton catalysis [85] Copyright RSC Adv., 2010 d). sonopiezocatalysis. reproduced with permission from the reference [54] copyright ACS, 2024.

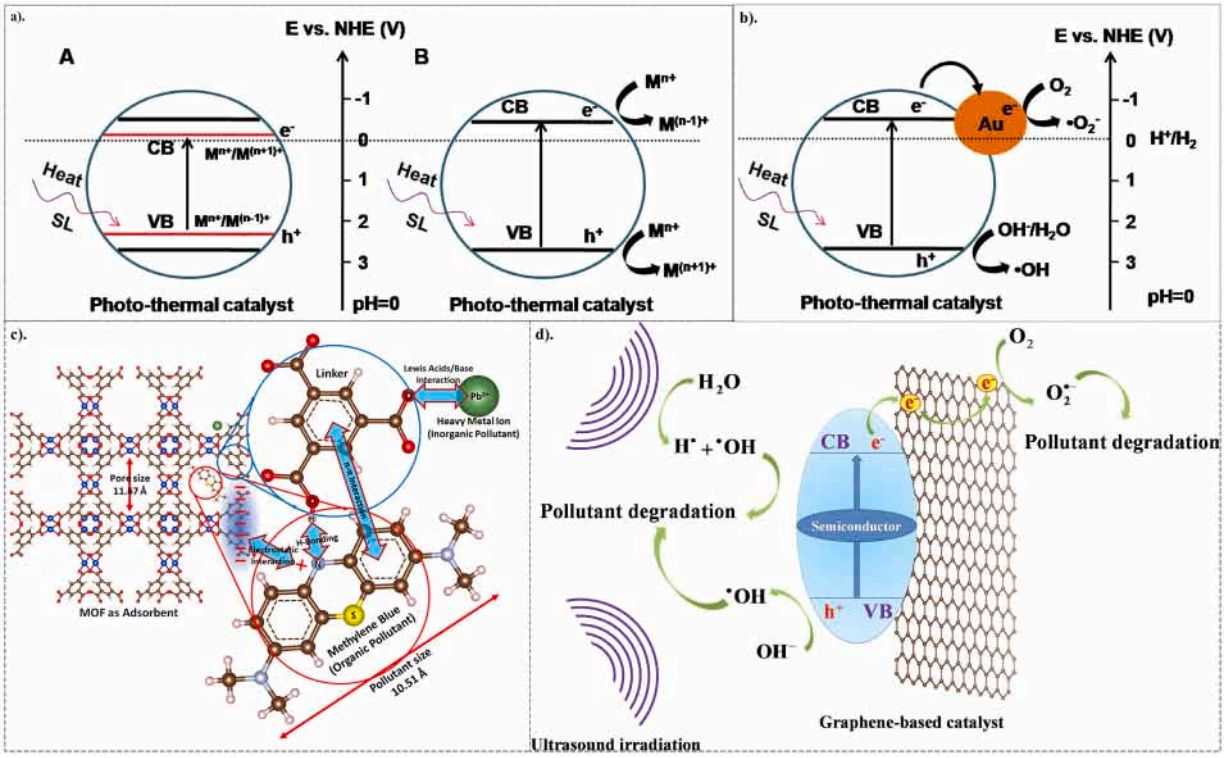

Fig. 8. a). Part A and B Schematic illustration for transition metal ions doped potothermal catalyst. b). Schematic illustration of the mechanism of Au-loaded TiO2. c). schematic illustration of degradation by MOFs of the organic pollutant via three different mechanisms. d). Schematic illustration of heterogeneous graphene-based sonocatalysis. Reproduced with permission [7,49,102] copyright Elsevier 2018, 2022, 2019.

3.1.1. Critical analysis of energy band theory in sonocatalysis

Sonocatalyst tests have been conducted on almost all photocatalysts. Typically, TiO_2 performs better sonocatalytically than other semiconductor photocatalysts [7]. But most of the time efficiency of the same catalysts, under ultrasound irradiation and UV/visible-light irradiation, differs, and for a few catalysts, it differs significantly [86–88]. Even the polymorphs of TiO_2 (anatase, rutile, and brookite) have distinct efficiencies when irradiated sonocatalytically as well as photocatalytically. Tayade et al. [89] synthesized rutile and anatase TiO_2 nanoparticles (NPs) and compared the degradation efficiency of the following four substrates under ultraviolet (UV)/visible light, i.e, Acetophenone, Nitrobenzene, Methylene blue and Malachite green. For each substrate, the activity of anatase TiO_2 was superior to that of the rutile TiO_2 [89]. Furthermore, it is a known fact that in the photocatalytic process, the anatase polymorph of TiO_2 typically shows greater activity than the rutile one [90–96]. On the other hand, sonocatalysis has contrary results. Wang et al. [64] examined how differently methyl Orange (MO) degraded when anatase and rutile TiO_2 NPs were present. They discovered that the rate of sonocatalytic degradation of rutile TiO_2 NPs' was roughly five times greater than that of the anatase ones.

Similarly, numerous studies have demonstrated that the same catalyst can exhibit markedly different efficiencies under UV/visible-light irradiation compared to ultrasound irradiation [87,97–100]. Notably, several reports have revealed substantial disparities between the photocatalytic and sonocatalytic performance of identical materials. For instance, Mogaddas et al. [101] showed that ZnO-based catalysts exhibited superior activity under UV irradiation relative to ultrasound. In a comparative investigation of iron-doped ZnO allotropes, Chakma et al. [86] explicitly noted that, "Without an external UV source, the sonoluminescence, light emitted during transient cavitation, cannot activate the photocatalyst." In contrast, other studies demonstrated the pronounced superiority of ultrasound. For example, ZrO_2 was employed to degrade both cationic and anionic dyes, where the degradation rate of Victoria blue under ultrasound was 34-fold higher than under light irradiation; similarly, sonocatalysis enhanced the degradation of direct red dye by a factor of 47 compared to photocatalysis [88]. Another study presented by Shankar et. al., utilizing sonocatalysis and sonophotocatalysis using pure and Fe-doped ZnO [86]. Although Fe-doping effectively lowered ZnO's bandgap, increasing its intrinsic photocatalytic activity and extending its light absorption into the visible spectrum, this electronic structure advantage did not result in a beneficial synergy when paired with ultrasound. According to the energy band theory, sonocatalysis should perform better when the bandgap is tuned, especially when combined with the UV light and sonoluminescence. However, the experimental results consistently showed a significant negative synergy. The author clearly stated that the expected activation of the photo-catalyst by sonoluminescence light does not occur.

Although numerous studies have attempted to explain the superior photocatalytic efficiency of anatase TiO_2, [90,95] no general or comprehensive investigation has addressed the underlying reasons for the differing efficiencies of the same catalysts under various irradiation conditions. This gap largely stems from the inherently complex nature of acoustic waves and their multifaceted effects in aqueous media. Therefore, more comparative studies on the fundamental mechanisms of photocatalysis and sonocatalysis are urgently needed. These variations in efficiency suggest the involvement of distinct mechanisms in ultrasound-driven processes. Nevertheless, sonocatalysis has often been interpreted through the lens of traditional photocatalysis, despite the fundamentally different natures of the two modalities. Electromagnetic radiation (light) and mechanical waves (sound) differ significantly in their physical and chemical interactions with aqueous media. While light waves decelerate in water, sound waves propagate approximately ten times faster. This contrast highlights that pressure waves, i.e., sound waves, interact with matter through unique pathways, distinct from those governed by electromagnetic radiation.

3.2. Fundamental mechanism of sonoadsorption

The underlying concept behind sonoadsorption is the special qualities of adsorbent materials and the acoustic cavitation produced by ultrasound work in conjunction. Although the process is started by localized high temperature (>5000 K) and pressure (>1000 atm) produced by acoustic cavitation, the formation, growth, and violent collapse of microbubbles, adsorbent materials play a role that goes beyond simple nucleation sites. Through a variety of mechanisms, such as bandgap engineering, adsorption-concentration effects, and electron transfer facilitation, these materials specifically increase the degradation efficiency [103–105]. The energy threshold for cavitation bubble formation is lowered by the heterogeneous surfaces offered by sonoadsorbents, such as activated carbon (AC) [106,107], biochar (BC) [108,109], alumina [110,111], zeolites [112,113], and few metal-organic frameworks (MOFs) [114]. Furthermore, other adsorbents have also been shown to exhibit improved adsorption of organic pollutants via ultrasound [115].

The key to adsorbent-based sonocatalysis is the transformation of ultrasonic energy into chemical energy through complementary electrochemical (charge separation, bandgap modulation) and physical (cavitation, adsorption) processes. Despite demonstrating successful synergistic effects, adsorbent-material-based sonocatalysis faces several limitations, chief among them being cost. Materials such as carbon nanotubes (CNTs), though effective, are unsuitable for large-scale wastewater treatment due to their complex and costly synthesis processes. Even biochar requires activation procedures, which raise costs, despite being less expensive. MOFs also face limitations in their low hydrothermal/chemical stability; many of them, particularly ZIF-8 and MOF-5, break down quickly in water or humid environments because metal-ligand bonds hydrolyze, collapsing their porous structure and releasing harmful metal ions (like Zn^{2+} and Cr^{3+}) into treated water [116,117]. Catalyst recovery comes next. It is difficult to filter out nanopowders that disperse in water, such as CNTs or g-C_3N_4 [103]. Although magnetic composites are beneficial, they also present new issues, such as iron leaching. Reusable catalysts lose 5–15 % of their efficiency per cycle, which is significant for continuous operations. Requires optimal conditions for operations such as pH, power, and frequency. The ideal ultrasonic frequency varies depending on the catalyst. It is very difficult to discern between catalytic and adsorption contributions (for example, AC adsorbs 50 % of pollutants prior to sonolysis) [107].

3.3. Sono-Fenton catalysis

The Sono-Fenton process is a sophisticated oxidation method that improves the breakdown of persistent organic pollutants in wastewater by combining the Fenton reaction (Fe^{2+}/H_2O_2) with ultrasound (sonolysis). The mechanism starts with ultrasonic cavitation, which creates extreme localised conditions (~5000 K, ~1000 atm) by using high-frequency sound waves to create microbubbles that grow and violently collapse. In addition to dissociating water molecules into atomic hydrogen (H·) and highly ·OH, this cavitation encourages the radical recombination that produces H_2O_2. Concurrently, the classical Fenton reaction takes place, in which Fe^{2+} catalyses the breakdown of H_2O_2 to generate more ·OH radicals, oxidising organic pollutants into simpler intermediates, CO_2, and H_2O. The ultrasonic-enhanced regeneration of Fe^{2+} from Fe^{3+}, which maintains the Fenton cycle and lowers the formation of iron sludge, is a significant benefit of this hybrid process. Microturbulence and shockwaves, two mechanical effects of cavitation, also enhance mass transfer, resulting in improved reactant dispersion and catalyst surface refreshment [118,119].

4. Piezo catalysis

Piezocatalysis is a technique that leverages mechanical energy, such as vibration, ultrasonic irradiation, or mechanical stress, and converts it into chemical energy to drive a range of reactions, including organic synthesis, water splitting, and the degradation of environmental pollutants, etc, utilizing mechanical tools such as ultrasound [120–123]. Piezocatalysis makes use of materials' intrinsic piezoelectric qualities of crystals that are non-centrosymmetric; these materials produce electric fields when mechanically deformed [99,124].

There is a lack of a unified framework in peizocatalysis, because of its interdisciplinary nature. It crosses the boundaries of solid-state physics, electrochemistry, and materials science. Results from early research were frequently interpreted using one perspective without considering the other. For instance, Results were explained on the basis of energy band theory by researchers working with piezotronics and photocatalysis for materials that resemble semiconductors, such as ZnO and MoS_2 [120,125]. Polarization screening was the focus of ferroelectric experts. Insulating ferroelectrics, such as $BaTiO_3$, were explained with the screening charge effect, which is dominated by surface ion dynamics [126–129]. Over time, the coexistence of the two mechanisms persists because each captures a distinct aspect of the piezocatalytic phenomenon.

4.1. Energy band theory

The energy band theory, while conceptually derived from piezotronics and photocatalysis, is distinguished by the pivotal role of electron transfer via mechanical strain in the energy band gap [130]. When a mechanical strain is induced a piezopotential across the material is formed, which tilts the bend of the piezoelectric material, resulting in a polarization of the material. Piezo-potential can lower the conduction band (CB) to a level below the electrolyte's highest occupied molecular orbital (HOMO) in the solution. As a result, the electrons move easily from HOMOs to CB. The electrons in the valence band (VB), on the other hand, leave the band and move into the lowest unoccupied molecular orbital (LUMO) of the electrolyte [131]. This process creates non-harmful species by breaking the bonds of the electrolyte. There are two possible ways in which band tilting can occur in energy band theory [132]. (1) Piezo catalyst uses mechanical energy to either directly excite electrons or (2) mobilize intrinsic charges within the material that arise from defects [133,134]. Periodic mechanical stimulation is necessary to sustain the piezopotential, which can guarantee the continuous band manipulation to avoid the depolarization field (Fig. 9a) [132,133,135].

When the catalytic process in energy band theory starts with the piezopotential being induced by mechanical strain provided by the cavitation collapse near the surface of the catalyst which provides high pressures, that tilt the bend structure of the piezoelectric material, followed by the generation of electron-hole pair, to permit redox reactions, this whole process is sometimes refers to as sonopiezocatalysis (Fig. 7d) [136] (Table 1).

4.2. Screening charge effect

The non-centrosymmetric crystal structures of piezoelectric materials produce a polarization field under mechanical strain [148,149]. This polarization field can also be produced by a temperature gradient, which results in bound charges at the material's surfaces [130]. The produced polarization fields can be either localized polarization fields in submicron domains (Fig. 10a) or the overall bulk polarization of the material called the top-to-bottom approach (Fig. 10b). Compensating charges, also known as screening charges, are drawn in from the surrounding medium, such as ions or electrons in an electrolyte, to counteract this polarization. The dynamic nature of this screening process is crucial for catalysis because, as mechanical strain varies (for example, through ultrasonication), the polarization field alternately gets stronger and weaker, which causes screening charges to adsorb and release cyclically. ROS are produced by this ongoing exchange and take part in redox reactions at the material's surface. Fig. 9(b) [150,151]

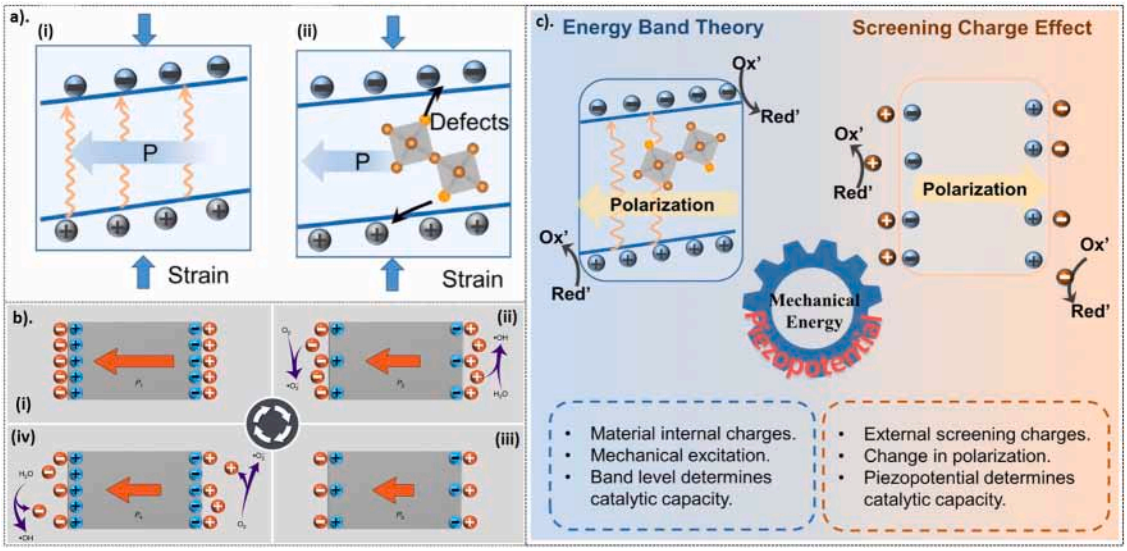

Fig. 9. Schematic illustration of a). The energy band theory (i) shows the direct band tilting from mechanical stress (ii) the defects in the material provides enough charges to generate band tilting. b). Screening charge effect in piezocatalysis. (i) Mechanical force induced polarization and electrostatically balanced state under stress. (ii) Surface redox reactions are triggered by the release of surface screening charges under compressed strain. (iii) balanced state under strain. (iv) polarization returns and so does the screening charges to drive reactions. Reproduced with permission from the reference [152] copyright springer nature. c). Differences in both mechanisms. reproduced with permission from the reference [10] copyright Wiley-VCH (part of John Wiley & Sons), 2022.

Table 1
The coefficients of piezoelectric materials arranged from high to low with their energy band gap.

Piezoelectric Material	Piezoelectric Coefficient (Pc N^{-1})	Band gap (eV)	References
Lead zirconate titanate (PZT)	593	3.05	[137,138]
Potassium sodium niobate (KNN)	230	1.75	[139]
$BaTiO_3$	190	3.18	[140]
Diphenylalanine (FF)	80	4.6	[141]
Polyvinylidene Fluoride (PVDF)	23	7	[142]
Cellulose	20	6	[143]
Chitosan	19	5.5	[144]
ZnO	13	3.2	[140]
Aluminum nitride (AIN)	6	6.1	[145]
Glycine polyvinyl alcohol (PVA)	5	5	[146]
Quartz (single crystal)	2.3	9	[147]

Note: The piezoelectric constants are mostly d_{33}; both piezoelectric constants and band gap values are approximate and can vary depending on factors such as synthesis methods and measurement conditions.

4.3. The governing mechanism of piezocatalysis: A critical debate

A thorough review that methodically presented both of these mechanisms from their inception to their current state was presented by Kai et al. in 2022. They also raised a few questions that helped to spark the never-ending discussion of the fundamental piezocatalysis argument; In what precise way is piezocatalysis initiated by the mechanical strain? Or is it really mechanical strain? [10] First, as the temperature gradient in the piezoelectric material is also capable of inducing polarization in the piezoelectric domains, it is highly likely that the generation of hotspots and shockwaves around the surface of the catalysts can also be a source of induced polarization, as well as the activation of catalysts. More experimental and theoretical understanding is required in order to know which effects overcome in activating the catalyst. Secondly, they emphasized the fact that if the energy band theory is the driving force behind the polarization of the catalyst, then a straightforward relationship between the material's band gap and efficiency should form. Third, the process is primarily driven by the piezopotential created within strained materials in both theories. Energy band theory states that the piezopotential improves reaction kinetics by influencing the semiconductor's band structure. On the other hand, the screening charge effect theory suggests a direct role, in which the catalyst's basic capacity to drive a chemical reaction is determined by the piezopotential itself reaching a magnitude large enough to directly initiate redox reactions. Both of these theories, therefore, contrast each other on the very basic level, yet neither of them has any material nor reaction distinctions.

Continuing the debate, in 2022, Bößl and Tudela list some factors that were necessary to account in order to understand the true process of piezocatalysis [153]. They highlight the fact that many studies overlook critical elements that are essential for optimising the piezocatalytic process. Despite the fact that many studies used the material at the submicron level, piezoelectricity practices dictate that the piezoelectric effect must increase with the length of the piezoelectric material [154]. Most studies do not report adsorption-desorption equilibrium, [129,149,155,156] band gap and piezoelectric strain coefficient (d_{33}), [127] which are important aspects in order to know whether the observed efficiency is due to the piezocatalytic effect or not. They further highlighted that to truly determine the piezo-catalysis efficiency, control experiments involving both poled and unpoled materials must be conducted [8]. The screening charge response of the material was the driving force behind most of the investigations, but still, energy band theory was presented to explain events where the potential band gap difference was insufficient [14]. If bulk polarization were the primary mechanism, larger particles (tens to hundreds of microns) would be needed to generate a significant piezoelectric output at these frequencies; nevertheless, the piezoelectric community has always utilized nanoparticles [153,154].

Although the same author Bößl et. al. did carried out an excellent study to resolve the ongoing debate in 2023. Comparing three materials, ZnO, Barium Titanate ($BaTiO_3$), and potassium bismuth titanate-bismuth ferrite lead titanate (BF-KBT-PT), with the increasing piezoelectric effect and decreasing energy band gaps for the degradation of Rhodamine B (Rh-B). They concluded that the sonochemistry is also playing a major role as in the controlled experiment without any catalyst the degradation of the Rh-B was 50 %. They further concluded that both

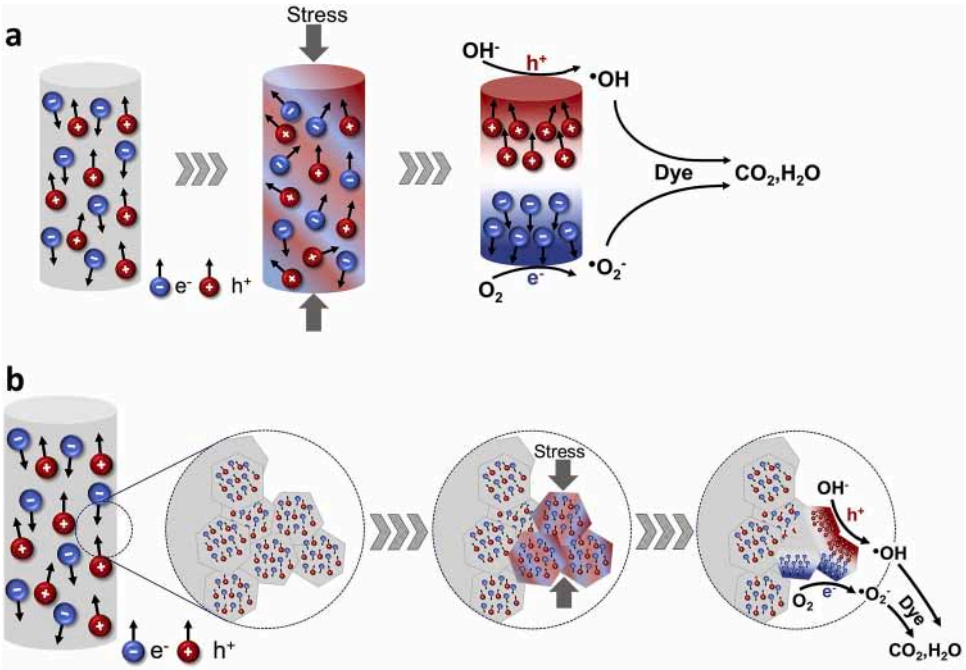

Fig. 10. An example of the various kinds of piezocatalytic mechanisms. a). the "top-to-bottom" electric potential difference caused by bulk polarisation of a piezocatalyst under stress. b). and the electric potential difference caused by localised polarisation within micro- and nano-structured features of piezocatalysts [153]. Copyright Elsevier, 2021.

the energy band theory and screening charge effect play a synergistic role, because the higher degradation was obtained by $BaTiO_3$, following the order $BaTiO_3$ (73 %) > BF-KBT-PT (61 %) > ZnO (59 %). Although, there were a few important facts and parameters that should have also been taken into account. Rh-B is a cationic and basic dye which shows some how considerable degradation via sonolysis alone, but other dyes like MO show almost negligible degradation [157–159]. Why few cationic dyes degrade to a considerable extent via acoustic cavitation alone, while others do not, is still an open question that lies at the heart of sonolysis and needs the attention of the research community. Furthermore, the optimal frequencies and powers of the catalysts were not taken into account. It was not clearly mentioned whether the pressure and frequency induced by the acoustic cavitation were sufficient enough to harness the full polarizability of BF-KBT-PT. In future such studies on the fundamentals are advised to first fully optimize the power and frequency of the ultrasound within the range where mechanical effects are fully harnessed and optimized with minimal chemical effects, to maximize the catalyst polarizability in order to evaluate its piezocatalytic activity. The radical scavengers test was also not conducted, although the author highlighted that there is a high possibility that different amounts of radicals will be formed via each catalytic path. Only one application of catalysis i.e, via degradation of dyes, the fundamental mechanistic debate can not be closed and stated. Other applications, such as metal reduction, water splitting, production of H_2O_2, etc must also be taken into account as catalysis is not limited to dye degradation only. Although, this study was not able to close the debate, it somehow showed that none of the catalysts under ultrasonic irradiation followed the band potential or Energy band theory and neither respected the piezoelectric coefficient nor a significant increase in efficiency of poled $BaTiO_3$ and BF-KBT-PT appeared. A slight decrease in the efficiency of a poled version somehow showed that the polarization indeed increases the efficiency of the catalyst. But if the polarization is a major contributor, keeping the mechanisms in mind, the poled versions should have had a considerable increase in efficiency than unpoled. However, the mechanism is still under debate. This study is indeed one of its kind that attempted to resolve the ongoing debate further; such studies can be a considerable progress [140].

Chirag et. al. (2024) presented a promising study to understand whether it is a material bulk polarization or surface polarization that is effective in catalyzing reactions [160]. They polished the unpoled $BaTiO_3$ surfaces and observed the 75 % decrease in the methylene blue degradation, stating that surface polarization indeed plays a significant role because the reannealing of the same surface restored the catalytic ability, favoring the screening charge mechanism by highlighting the role of surface charges.

Recently, an excellent review on organic synthesis via ball milling catalyzed reactions by Carlos C. et. al. (2025) appeared, in which they doubted the overall credibility of piezo catalysis [161]. They presented a series of contradictory experimental results challenging the straightforward assumption that a material's piezoelectric strength directly dictates its catalytic performance. The behavior of perovskite-structured titanates, such as $BaTiO_3$, is a major mystery [162]. These materials are great candidates for proof-of-concept studies because they are highly tunable and easily synthesized, but their catalytic activity does not always match their piezoelectric characteristics. For example, in a number of organic reactions, such as arylation and cyclization, the cubic phase of $BaTiO_3$, which is piezoelectrically inactive because of its high symmetry, has demonstrated surprisingly high activity [121,163,164]. In contrast, the traditional, piezoelectrically active tetragonal phase performs significantly better in other reactions, such as trifluoromethylation. This discrepancy implies that there is a complex and nonlinear relationship between crystal polarity and catalytic activity. Their further discussion about the diverse performance of other materials emphasizes this complexity even more. Piezoelectric material ZnO exhibits high activity in one kind of reaction but poor performance in others [165]. This suggests that catalytic success varies depending on the type of reaction and is not a general characteristic of a good piezoelectric material. The findings that non-piezoelectric materials, with centrosymmetric crystal lattice like TiO_2, can also demonstrate catalytic activity in specific mechanoredox reactions pose the biggest obstacle to the fundamental theory [63,165]. Additionally, semiconductor energy band theory, which is essential to photocatalysis, appears to be less predictive in this situation. Despite having stronger redox potentials than $BaTiO_3$, materials such as lithium niobate ($LiNbO_3$) are typically less active,

suggesting that the energy levels alone cannot be the only factor driving the reactions [166]. Since conventional measures of piezoelectric performance, like the piezoelectric coefficient (d_{33}) and energy band levels, seem to be ill-suited for forecasting catalytic activity. The fundamental assumption that the piezoelectric effect is the main driver is seriously called into question by the finding that non-piezoelectric substances can still drive reactions and that the piezoelectrically inactive phases of materials can perform better than their active counterparts. This basic discrepancy raises questions about whether "piezocatalysis" is a unique and legitimate mechanism or just an effect that has been misattributed.

Another recent study to understand the mechanism of piezo catalysis published in 2025 by Lishang et. al [167]. They utilized two different-sized less than $1\mu m$ *and* $10-15\mu m$ $BaTiO_3$ nanosheets. Identical material of different sizes were utilized in order to keep the energy band gap same. They hypothesized that if the band gap is responsible for the observed catalysis, then both particles must perform identically. On contrary, the sample with the lower piezopotential (small nanosheets) performed noticeably better than the one with the higher piezopotential (large nanosheets). The traditional energy band model, which holds that a stronger piezopotential should better bend bands and drive internal charge carriers, is called into question by their findings. They further explained that in order to adsorb and desorb external screening charges, the piezopotential primarily functions as a dynamic switch that alternates quickly. The pivotal role of these screening charges is emphatically highlighted by the dominance of superoxide radicals ($\cdot O_2^-$), whose generation was drastically amplified under control ultrasound and light, as well as combined catalysis. Since $\cdot O_2^-$ is formed directly from adsorbed oxygen molecules capturing electrons, its prevalence confirms that the reactive charges are predominantly these externally sourced, piezopotential-switched screening charges, rather than the material's internal band bending, solidifying the screening charge model as the core mechanism.

These results raise serious questions about the credibility of piezocatalysis. Not only are the non-centrosymmetric materials active in ball milling, but such results of their activeness can also be found via ultrasound. Some recent studies showed the remarkable degradation of pollutants via ultrasound by non-centrosymmetric crystals such as; hydroxylapatite ($Ca_{10}(PO_4)_6(OH)_2$), [168,169] bismuth ferrite, [170] Calcium Titanate ($CaTiO_3$), [171] zinc hydroxystannate (ZHS) [172]. Although for each material whether it is centrocemitric or not the efficiency of the catalyst has always found to be increased by either changing or modifying their self-polirization, [157,160,173,174] annealing, [175,176] adding the dopants, [177–179] adjusting the carrier concentrations, [180,181] or combining with different materials to form heterojunction but a consistent inconsistency has been observed in literature according to the piezoelectric coefficients and energy band gaps across various materials. The aforementioned studies unequivocally and critically demonstrate how energy band theory falls short in describing catalytic performance. The theory of surface screening charges is unable to explain the exceptional catalytic performance of non-centrosymmetric materials because of its reliance on piezopotential, which also shows ambiguities when compared with the size. This fact also necessitates more thorough experimental and theoretical research, but it somehow manages to explain surface chemistry.

5. Contact-Electro-Catalysis (CEC)

If toxic reagents are employed in conjunction with microwaves or ultrasonics, and the subsequent separation and purification steps require substantial amounts of volatile organic solvents, the overall process cannot be considered environmentally benign. In such cases, the inherent advantages of these alternative activation methods are effectively nullified. It was not until 2022 that pristine dielectric materials were utilized for the treatment of contaminated water (degradation of dyes) via ultrasound [24]. Later, by the use of the same pristine dielectrics, degradation of dyes could also be realized through ball milling and flow electrification in dielectric tubes [182,183].

This advancement of utilizing pristine dielectrics has its roots in the 21st century, with the dawn of major advances in triboelectrification [1]. Major scientific achievements and scientific terms emerged, one of which includes triboelectric nanogenrators (TENGs) and contact electrification (CE) regained its attention, which includes charge transfer on contact, and friction is not necessary in CE [184–186]. CE can occur between solid, liquid, and gas, excluding the phase of matter [184,187,188]. The advancement in CE and the scientists' urge to harness the full potential of triboelectric materials, and when they come in contact with liquids, paved the way towards solid-liquid contact electrification, which further led to the discovery of CEC [9,187]. Now, CEC is known as a safer, profound, non-volatile, non-toxic, highly durable technique with the ability to work in extreme temperatures and pressures, derived by the mechanism of CE [9]. CEC has gained wide popularity in recent years, and ultrasound, being one of the ways to initiate contact between solid dielectrics and liquid, often been misinterpreted with sonochemistry and sonocatalysis. This review is an attempt to highlight the unique fundamental mechanism of CEC, from other catalytic processes that utilize ultrasound. For a detailed discussion about the role and significance of CEC, some excellent reviews are already available in the literature [1,9,189–193].

5.1. Fundamental mechanism of CEC

CEC is an interfacial mechanism that takes place between two surfaces, those surfaces can be solid and liquid, solid and gas, or liquid and liquid etc., initiated by mechanical forces; therefore, the fundamental mechanism of CEC involves several steps. The first step involves CE between the dielectric and solvent. The solid dielectric (mostly with high electronegativity) comes into contact with the solvent to the extent that their electron clouds overlap, and an electron is transferred from the liquid to the solid. This contact separation cycle ensures the transfer of electrons. In the second step, the charged solid surface, under the action of mechanical force, drives redox reactions near the interface. This step involves the subsequent production of ROS that further accelerates chemical reactions. This second step forms the foundation of the CEC process [9,194].

5.2. Electron transfer during CE

Various theoretical and experimental studies have explained electron transfer during CE. Triboelectric nanogenerators and controlled droplet-film interactions are used in experiments to show that polymers such as polytetrafluoroethylene (PTFE) can accumulate electrons from water, with charge transfer being influenced by functional groups and ion concentration [195–198]. These results are supported by theoretical models that demonstrate electron redistribution at interfaces, such as quantum-mechanical and density functional theory calculations [199]. Furthermore, because of their spin-selective behavior and thermionic emission, thermal and magnetic investigations validate electrons as the primary charge carriers [184,200]. The basis for CEC, in which mechanical energy propels redox reactions via interfacial electron exchange, is this knowledge of electron transfer during CE.

The function of electron transfer is further supported by the fact that chemical reactions such as chemiluminescence are influenced by the polarity of electrified droplets [152,200–205]. The design of effective CEC systems is made possible by these insights, which also help to clarify CE mechanisms. The electron transfer process during CE closes the gap between basic phenomena and real-world applications by establishing electron transfer as the key to CE, paving the way for developments in catalytic strategies that make use of mechanical energy. Recently, Tang et al. [206] theoretically analyzed the impact of frontier molecular orbitals (FMOs) on CE between polymers and water. The study compares the vertical attachment energies (VAE) and lowest unoccupied molecular orbital (LUMO) levels of five polymers: PTFE, PVDF, polyvinyl

Chloride (PVC), polypropylene (PP), and Polyethylene (PE). According to the findings, polymers like PTFE that have lower LUMO levels perform better in CE because they can take electrons from water more easily. VAE calculations support this trend by showing that PE, which has the highest LUMO, requires much more energy (0.723 eV) for electron transfer than PTFE, which requires the least energy (0.087 eV), Fig. 11. Fig. 11c visually explains the charge transfer between water and a polymer.

5.3. Ultrasound-induced CE

Fig. 11d depicts a schematic of contact electrification using ultrasound. Cavitation bubbles generated by sound waves produce contact and separation cycles between solid and liquid (mostly water). These contact separation cycles result in the overlap of electronic clouds and electron transfer. FMOs influence this charge transfer. Molecules with lower LUMO and higher electronegativity have shown superior efficiency. Fig. 11c illustrates the suggested mechanism and breaks down the electron transfer process into three stages: a high energy barrier blocks electron exchange prior to contact; mechanical energy lowers this barrier during contact, enabling electrons to flow from water to the LUMO of the polymer; and following separation, electrons stay on the polymer and accumulate with repeated contact. These results provide a basis for the optimization of polymer selection in CE applications by highlighting the crucial role that LUMO levels play in CE efficiency [206] Fig. 11.

5.4. Contact-electro-catalysis

Fig. 11e illustrates the complete CEC mechanism. First CE between a liquid and solid dielectric under contact separation cycles charged the solid surface. Then, further mechanical contact between charged solid and liquid drives subsequent ROS, which accelerates chemical reactions. A thorough CEC process for generating ROS could be represented as illustrated in Fig.11f, which is exemplified by the CE-driven electron transfer between the FEP particles and the surrounding substrates.

The studies of interaction between triboelectric material and water show that when FEP comes into contact with water molecules, the water molecule becomes positively charged and loses its electron density and the triboelectric material will become charged i.e. FEP* [195,207,208]. Water molecules first become water radical cations after losing electrons; the lifetime of water radical is less than a picosecond; therefore, it will immediately combine with a water molecule, then a quick proton transfer produces hydronium cations and hydroxyl radicals [209–211]. According to ab initio molecular dynamic calculations, the water's hydrogen bond network may make it easier for protons and electrons to exchange during CEC [212]. To denote the charged state of FEP, the term FEP* is introduced. When O_2 molecules collide with FEP*, they absorb electrons from its surface, forming superoxide radicals and returning FEP to its initial uncharged state. As long as the mechanical stimuli are present, this cycle will continue. Using PTFE as an example Fig. 11g, details a more thorough two-step process for producing ROS via CEC. Initially, when H_2O and PTFE come into contact, electrons will be transferred from H_2O to PTFE, creating water radical cations. These will then undergo a quick proton transfer from water to hydronium cations and hydroxyl radicals. When they collide with sufficient energy, the electrons that have accumulated on the charged surface of PTFE* will be converted to dissolved O_2 molecules; this is known as the second step. After gaining these electrons, O_2 will be transformed into superoxide radicals, and PTFE* will return to its initial uncharged state. As

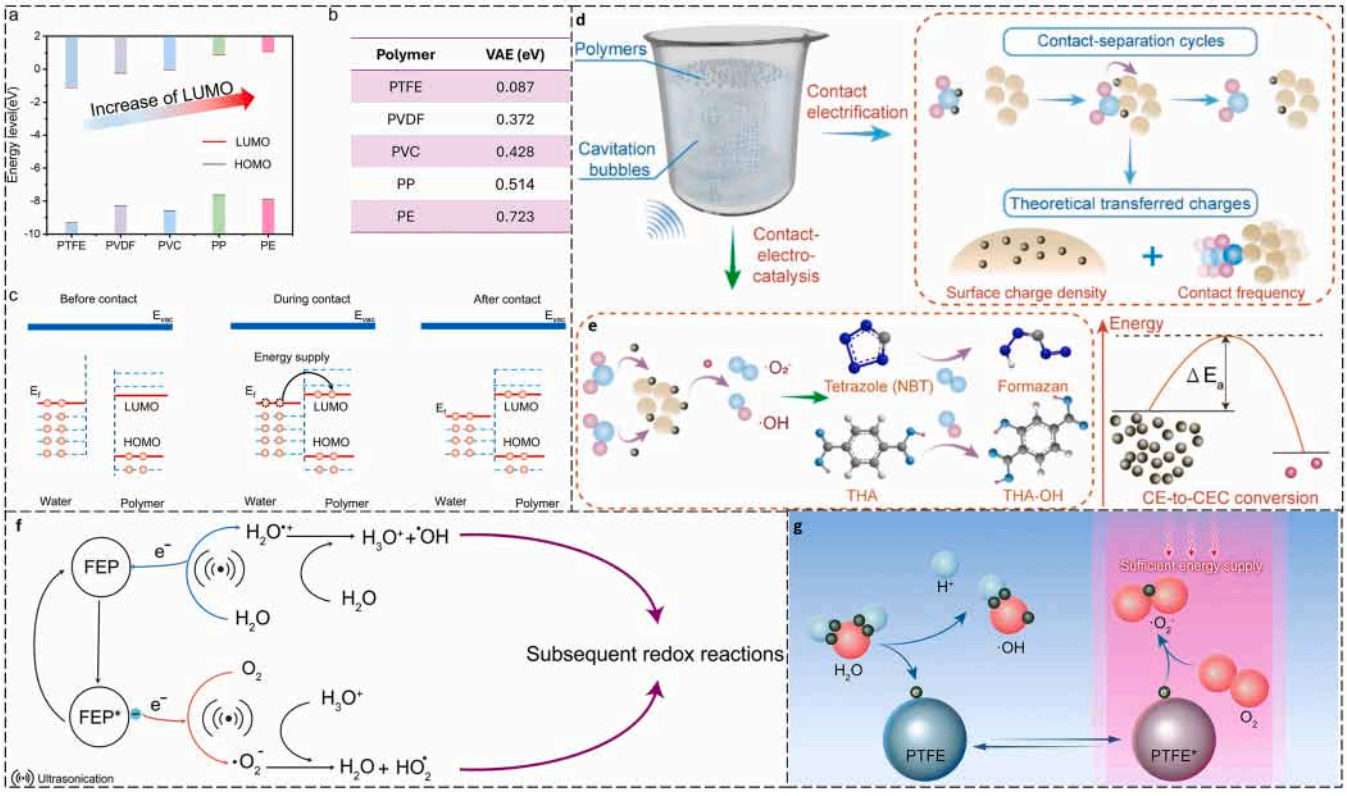

Fig. 11. Theoretical studies that show how different polymers' CE abilities vary. a). Energy levels of the frontier molecular orbitals of different polymers were calculated. (b) The various polymers' vertical attachment energy (VAE). (c) A suggested mechanism for the process of electron transfer between water molecules and polymers [206]. Copyright Materials Advances, 2024. d). Schematic of Contact electrification in ultrasound and the transfer of charge in the contact separation cycle. e). CE induced contact electro catalysis and production of ROS for redox reactions [194]. Copyright Elsevier, 2025. f). A particular CEC procedure that uses ultrasonication and FEP to produce ROS. g). suggested two-step process for using CEC to produce radical oxygen species [9]. Copyright Royal Society of Chemistry, 2024.

long as the mechanical stimuli are present, this cycle will continue [24,195,213,214] (Figs. 12 and 13).

5.5. Contact-electro-chemistry

An electric field will be produced in space by the charged surface caused by CE, and a strong electric field has the power to greatly alter the surrounding environment [216,217]. For instance, the electric field can alter the electronic structure or cause polarization in nearby molecules, which would alter their chemical activities [218,219]. Furthermore, charged species like electrons can be transported and diffused by the electric field at contact interfaces [220,221]. Additional research has demonstrated that by promoting electron transfer, an increased electric field at interfaces may result in a faster reaction rate [222]. These experimental findings provide more evidence that CE may stimulate chemical reactions. CEC, which connects mechanochemistry and CE, has been suggested as a major addition to current catalytic techniques [24,182].

CEC provides a vital link between the intended chemical behaviors of products and the intrinsic physical characteristics of reactants. Molecular structure, solid-liquid interface interactions, mechanical performance, and surface properties of the materials involved are some of the factors that start the process. By influencing charge transfer events at interfaces, these physical characteristics allow the system to use interfacial or mechanical forces for chemical activation. As the effects of CE spread, they make improvements possible in a number of important chemical areas. These include the production of free radicals, enhanced reaction rates, exact control over the course of the reaction, and the selective formation of desired products. The change represents a transition from mechanical and structural parameters to customized chemical results.

Therefore, Wei's group broadened the scope of CEC to a more general framework termed contact-electro-chemistry (CE-Chemistry), highlighting its ability to couple targeted physical interactions with chemical reactivity. This approach enables a variety of reaction pathways, including redox reactions, polymerization, and fluorescence generation, through CE-induced electron transfer [202,223,224]. Furthermore, Wei's team uncovered Janus chemical processes in CE-chemistry, particularly during oxygen reduction reactions, by correlating the standard electrochemical potentials with the electronegativity of dielectric materials [159]. The applicability of CE-chemistry was also extended to non-aqueous media, where systematic investigations revealed that the absence of an EDL markedly enhances CEC efficiency [159,215]. Generation of H_2O_2 via CEC has also been reported by many authors [212,214]. The efficiency of the generation of H_2O_2 even exceeds that of the photo and piezo catalysis [225] (Table 2).

5.6. A critical discussion on the foundations of CEC

The conventional methods used in their respective material fields

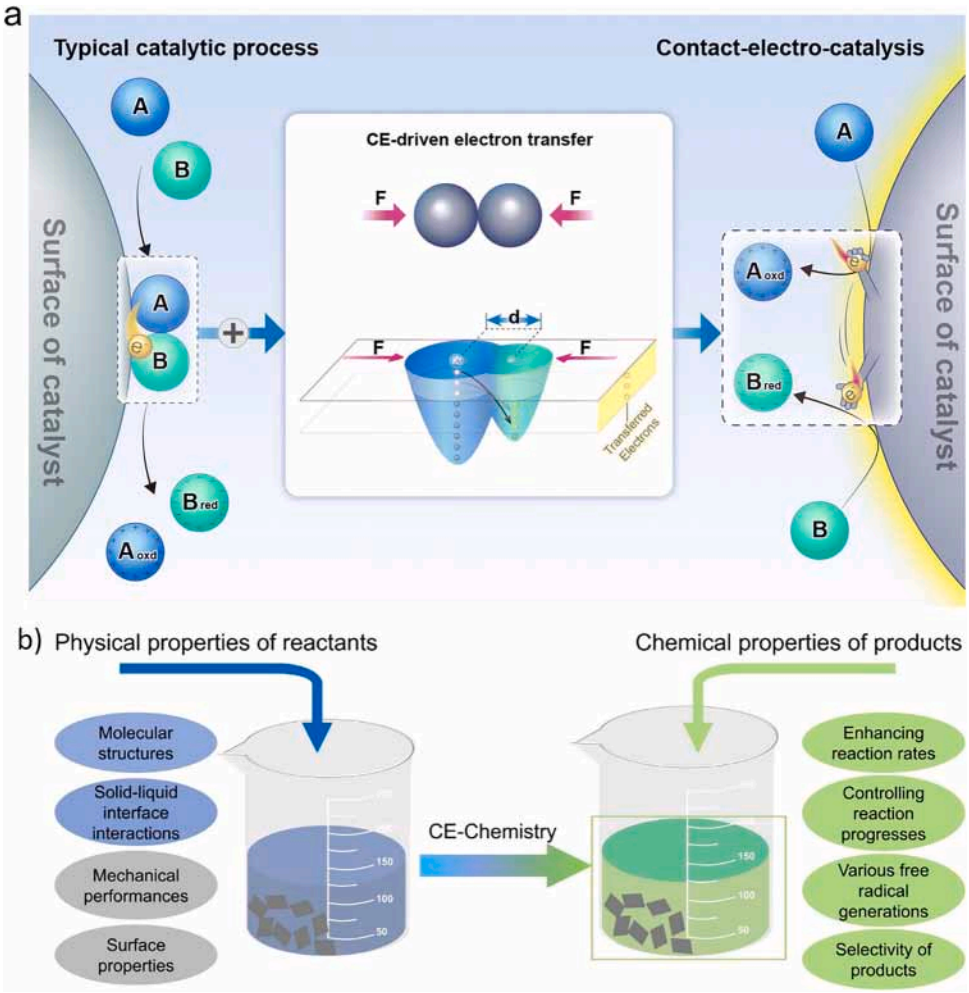

Fig. 12. a). Using the CE effect to drive electron transfer in a common catalytic process—where the "grab" and "release" of an electron from a water molecule are animated, contact electrocatalysis (CEC) was proposed. Reproduced with permission from the reference [9] Copyright Royal Society of Chemistry, 2024. b). A general schematic of CEC mechanical properties and applications [215]. Copyright by ACS, 2024.

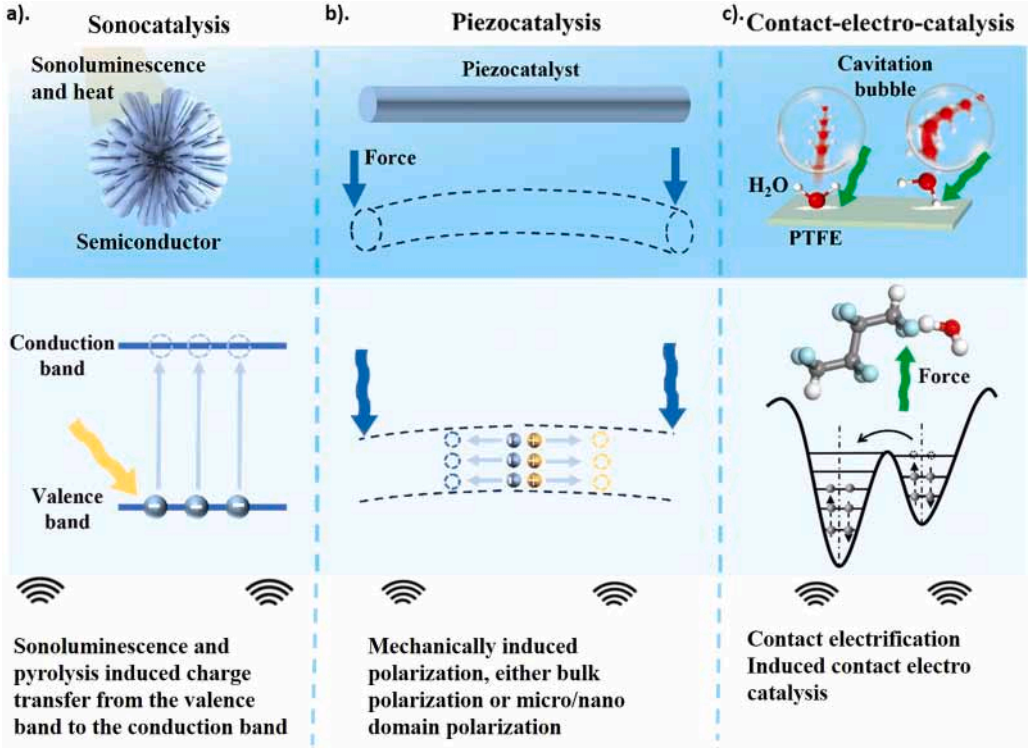

Fig. 13. Fundamental mechanisms of a) sonocatalysis b) piezocatalysis c) contact electro catalysis reproduced with permission from the reference [191] copyright Royal Society of Chemistry, 2024.

Table 2
Production of H2O2 with various catalysis mechanisms.

Production rate (μM h^{-1})	Flow Type	Catalyst type	Material	Reaction condition
1071	Continuous	CEC	PTFE particle	Ultrasound 40 kHz, 240W
310	Batch	CEC	PTFE particle	Ultrasound 40 kHz, 240W
260	Batch	CEC	PTFE stir bar	Ultrasound 40 kHz, 240W
390	Batch	Piezocatalysis	Bi12O17C12	Ultrasound 40 kHz, 100W
230	Batch	Piezocatalysis	BIO/FeIII	Ultrasound 40 kHz, 152W
80	Batch	Piezocatalysis	UBTO-0V2	Ultrasound 40 kHz, 300W
150	Batch	Photocatalysis	HCOF	Xe lamp;> 420 nm; 500W
810	Batch	Photocatalysis	Pd/A/$BiVO_4$	Xe lamp;> 420 nm; 0.4Wcm^{-1}
50	Batch	Photocatalysis	CTF-BDDBN	Xe lamp;> 420 nm; 44.5Wcm^{-1}

Reproduced with permission from [225]

and the attempt to explain catalysis using the same principles later led to experimental ambiguities, as we have seen previously for sonocatalysis and piezocatalysis. The same approach followed for CEC must also be called into question. For CEC, the studies of electron transfer from water to the dielectric in SL-TENGS are in full agreement with the efficiency of catalyzing reactions in CEC [195,208,226]. The electron transfer is not only limited to triboelectric materials; it is supported by many confined studies, which support that the electrostatic fields are a powerful yet underappreciated factor in catalysis. In confined environments such as zeolites, asymmetric charge distributions generate fields as strong as 10^9 V m^{-1}, comparable to those at solid–liquid contact electrification interfaces. These fields can polarize small molecules (e.g., H_2, CO_2), stabilize reactive intermediates, lower activation barriers, and modulate the electronic structure of catalytic metal sites. Through electronic confinement and field-induced polarization, they reshape reaction pathways, influence selectivity and diffusion, and couple thermodynamic and kinetic effects. Harnessing such interfacial electrostatic fields, without the need for complex nanostructures, CEC offers a broadly applicable strategy for field-enhanced catalysis [227,228].

However, there is no direct experimental verification for the hypothesized second step, in which dissolved oxygen from water can take an electron from the dielectric and reduce itself to $\cdot O_2^-$ radical. Conversely, the dielectrics that are positively charged in solid-solid CE remained negatively charged upon contact with water [195]. Additionally, a recent study by Peng et. al. about the generation of radicals with and without ultrasound in the solid-liquid CEC showed that the $\cdot O_2^-$ is only generated by ultrasound, while CEC performed without ultrasound only showed the generation of ·OH radicals [213]. This discrepancy in CE and CEC needs to be addressed. However, it does not mean that dumping anything into the ultrasound can generate radicals and catalyze reactions. Recently, Di Wei et. al. showed that the presence of glass balls along with FEP balls decreased the efficiency [159]. This proves that the surface chemistry plays an important role, as can be seen from the further studies by the same author, that the tuning of surface properties has highly increased the catalytic efficiency [228,229].

Although CEC claims to utilize all kinds of triboelectric materials, some studies even claim that, apart from triboelectric material, CEC is a universal process without its dependence on material; however, its efficiency is only restricted to a few polymers that contain the element fluorine [9]. Only a few triboelectric materials, such as FEP, PTFE, and PVDF, are catalytically active, which drastically reduces the CEC scope [206]. But unlike piezocatalysis, which becomes catalytically active in nano domains, CEC has performed remarkably well in both micro to mm scales, which emphasizes the fact that it is indeed a phenomenon that follows the principle of electronegativity, which comes into action via CE [215,230]. Yang et. al. did first-principles DFT calculations to explain solid-liquid CE [231]. DFT calculation showed a direct correlation between a polymer's charge transfer capability and its HOMO-LUMO gap. In this study, the precise

ranking that DFT reveals is complex. Because of its estimated wide band gap, PVDF was found to be the highest charge gainer in the simulations, following PTFE>PDMS>Nylon66>PET>PP>KEPTON. According to the calculations, the precise atomic-level configuration, which includes the position, geometry, and intricate bonding environments of the molecules in the model, as a significant impact on this electronic property. While experimentally, PTFE is more catalytically active than PVDF. The DFT results are no wonder because PVDF, being a piezoelectric material, has a more polarized structure than PTFE. However, its functional groups are less electronegative; therefore, it has less efficiency than PTFE. Below is the list of a few triboelectric materials in terms of their decreasing ability to gain electrons from water experimentally, according to the reference [195]. FEP > PTFE > PVDF > PE > PP > PVC

6. Conclusion and future perspective

Frequency is the most critical parameter governing ultrasound-driven catalysis. At low frequencies (20–100 kHz), ultrasonic waves primarily impart mechanical effects, such as particle fragmentation, enhanced mass transport, and interfacial activation, because the energy input is insufficient for direct bond cleavage. In contrast, higher frequencies (up to ~1 MHz) optimize conditions for chemical transformations via sonochemistry, where cavitation-induced phenomena drive bond-breaking reactions. When ultrasonic irradiation is applied across a broad range of frequencies and intensities in heterogeneous systems to accelerate chemical reactions, the process is termed sonocatalysis. Sonocatalytic activation mechanisms typically involve pyrolysis from transient cavitation, sonoluminescence, and adsorption-enhanced surface reactions, sharing conceptual parallels with photocatalysis. Distinct from these are mechano-driven catalytic processes such as piezocatalysis and contact-electro-catalysis (CEC), which exploit precisely tuned ultrasonic parameters to selectively harness mechanical energy and interfacial charge transfer rather than photochemical or thermal effects. Although both are mechanocatalytic, their activation mechanisms differ fundamentally: piezocatalysis arises from piezoelectric polarization under mechanical stress, generating screening charge effects, though its detailed mechanistic understanding remains under debate. In contrast, CEC uniquely relies on repetitive contact-separation cycles at liquid-solid interfaces to induce charge transfer via mechano-driven contact electrification, distinguishing it intrinsically from other ultrasound-activated catalysis. CEC also offers remarkable sustainability advantages, including catalyst recyclability without performance degradation and elimination of pollutant adsorption requirements. Across all ultrasonic catalytic approaches, CEC, piezocatalysis, and conventional sonocatalysis, the underlying mechanisms and efficiencies are highly material-dependent. The catalyst class (semiconductors, piezoelectrics, or dielectrics) and specific physicochemical properties govern the dominant reaction pathways, whether photo-thermal, adsorption-driven, piezoelectric, or CE. Notably, significant performance variability exists even within the same material class, underscoring the importance and need to understand mechanistic pathways in more detail for material design in optimizing ultrasound-driven catalytic efficiency.

A key question, whether the band structure, central to photocatalysis, also governs sonochemical and piezocatalytic efficiency, has now been addressed, where numerous studies have now highlighted the non-linear behavior of the piezoelectric coefficient, piezopotential, and energy band gap, in catalyzing reactions. While CEC remained successful in terms of the electronegativity of the functional groups. However, one trend has always remained the same in literature: increasing polarization, charge carriers, introducing dopants and forming hetrostructures of the material has shown increased activity, but no straightforward theory can be presented at this time that can fit different materials into one order according to their catalytic efficiency under ultrasound. The ongoing debate further showed that surface properties play an important role in catalyzing the reactions.

Future studies must focus on decouple mechanical and electronic contributions; systematic comparative studies are needed that apply fixed ultrasonic parameters across diverse material classes. Representative “star” materials from each class, such as TiO_2 (semiconductor), $BaTiO_3$ (piezoelectric), and FEP (dielectric), exhibiting superior catalytic performance, should be identified and investigated to elucidate the origins of their reactivity. Such comparative analysis could reveal fundamental design principles. Synergistic investigations integrating catalysis modalities, such as photo-CEC and thermo-CEC, are essential for deeper insight into catalyst activation pathways. Overall polarizability of the material combined with assessments of electronegativity, electron affinity, work function, and charge carriers may be able to clarify the mechanism. Developing hybrid mechanocatalysts that merge inorganic band engineering with organic HOMO-LUMO tuning (e.g., perovskite-organic composites) represents a promising frontier. Immediate priorities include resolving the carrier versus screening charge debate, expanding the spectrum of reactive radical species, and enabling real-time control of mechano-catalytic processes. Which can help towards the development of ultimately, constructing a unified framework that could help maps the material on the basis of their catalytic efficiency. More knowledge should be on which current knowledge base could facilitate convergence across CE, piezo, and sonocatalysis, unlocking the full potential of ultrasound-driven catalysis.

CRediT authorship contribution statement

Sidra Tul Muntaha: Writing – review & editing, Writing – original draft, Visualization, Investigation, Conceptualization. **Zhong Lin Wang:** Project administration. **Di Wei:** Writing – review & editing, Supervision, Resources, Project administration, Investigation, Funding acquisition.

Declaration of competing interest

The authors declare that they have no known competing financial interests or personal relationships that could have appeared to influence the work reported in this paper.

Acknowledgment

This work was supported by the National Natural Science Foundation (grant number 22479016).

Data availability

Data will be made available on request.

References

[1] S. Li, J. Liu, Z.L. Wang, D. Wei, Mechano-driven chemical reactions, Green Energy & Environment (2024).
[2] L. Takacs, The mechanochemical reduction of AgCl with metals: revisiting an experiment of M. Faraday, J. Therm. Anal. Calorim. 90 (1) (2007) 81–84.
[3] L. Takacs, M. Carey Lea, the first mechanochemist, J. Mater. Sci. 39 (16) (2004) 4987–4993.
[4] (1) Die chemische Literatur und die Organisation der Wissenschaft (2) The Foundations of Chemical Theory (3) Inorganic Chemistry, Nature 107 (2698) (1921/07/01) 613–615, 1921.
[5] D. Chen, S.K. Sharma, A. Mudhoo, Handbook on applications of ultrasound: sonochemistry for sustainability, CRC press, 2011.
[6] Q.T. Trinh, et al., Sonochemistry and sonocatalysis: current progress, existing limitations, and future opportunities in green and sustainable chemistry, Green Chemistry (Easton) (2025).
[7] P. Qiu, B. Park, J. Choi, B. Thokchom, A.B. Pandit, J. Khim, A review on heterogeneous sonocatalyst for treatment of organic pollutants in aqueous phase based on catalytic mechanism, Ultrason. Sonochem. 45 (2018) 29–49.
[8] F. Bößl, T.P. Comyn, P.I. Cowin, F.R. García-García, I. Tudela, Piezocatalytic degradation of pollutants in water: importance of catalyst size, poling and excitation mode, Chem. Eng. J. Adv. 7 (2021) 100133.
[9] Z. Wang, X. Dong, W. Tang, Z.L. Wang, Contact-electro-catalysis (CEC), Chem. Soc. Rev. 53 (9) (2024) 4349–4373.

[10] K. Wang, C. Han, J. Li, J. Qiu, J. Sunarso, S. Liu, The mechanism of piezocatalysis: energy band theory or screening charge effect? Angew. Chem. Int. Edn. 61 (6) (2022) e202110429.
[11] B. Chen, et al., High tribocatalytic nitrogen fixation on friction interface of SrTiO3 non-piezoelectric nanosheets and PTFE, Surfaces and Interfaces (Providence) (2025) 106461.
[12] T. Li, W. Hu, C. Tang, Z. Zhou, Z. Wang, L. Shu, Enhanced piezo-catalysis in ZnO rods with built-in nanopores, J. Adv. Ceram. 12 (12) (2023) 2271–2283.
[13] S.A. Asli, M. Taghizadeh, Sonophotocatalytic degradation of pollutants by ZnO-based catalysts: a review, ChemistrySelect 5 (43) (2020) 13720–13731.
[14] A. Siddique, et al., PVDF-based piezo-catalytic membranes—A net-zero emission approach towards textile wastewater purification, Polymers (Basel) 16 (5) (2024) 699.
[15] E.Carr Everbach, Medical diagnostic ultrasound, Physics (College Park Md.) Phys. Today 60 (3) (2007) 44–48.
[16] O. Darrigol, The analogy between light and sound in the history of optics from the ancient Greeks to Isaac Newton. Part 2, Centaurus 52 (3) (2010) 206–257.
[17] D. Peters, Ultrasound in materials chemistry, J. Mater. Chem. 6 (10) (1996) 1605–1618.
[18] J. Bamber, M. Tristam, Diagnostic ultrasound. The physics of medical imaging, 1988, pp. 319–388.
[19] G. Leventhall, What is infrasound? Prog. Biophys. Mol. Biol. 93 (1-3) (2007) 130–137.
[20] T.G. McKenzie, F. Karimi, M. Ashokkumar, G.G. Qiao, Ultrasound and sonochemistry for radical polymerization: sound synthesis, Chem. Eur. J. 25 (21) (2019) 5372–5388.
[21] G.t. Haar, Ultrasound bioeffects and safety, Proc. Inst. Mech. Eng. Part H J. Eng. Med. (Baltimore) 224 (2) (2010) 363–373.
[22] W. H. Organization, Training in diagnostic ultrasound: essentials, principles and standards: report of a WHO study group (no. 875), World Health Organization, 1998.
[23] R.J. Wood, J. Lee, M.J. Bussemaker, A parametric review of sonochemistry: control and augmentation of sonochemical activity in aqueous solutions, Ultrason. Sonochem. 38 (2017) 351–370.
[24] Z. Wang, et al., Contact-electro-catalysis for the degradation of organic pollutants using pristine dielectric powders, Nat. Commun. 13 (1) (2022) 130.
[25] S. Merouani, A. Dehane, O. Hamdaoui, Ultrasonic destruction of surfactants, Ultrason. Sonochem. (2024) 107009.
[26] W.T. Richards, A.L. Loomis, The chemical effects of high frequency sound waves I. A preliminary survey, J. Am. Chem. Soc. 49 (12) (1927) 3086–3100.
[27] F. Schmitt, C. Johnson, A. Olson, Oxidations promoted by ultrasonic radiation, J. Am. Chem. Soc. 51 (2) (1929) 370–375.
[28] K.S. Suslick, Sonochemistry, Science (1979) 247 (4949) (1990) 1439–1445.
[29] E.B. Flint, K.S. Suslick, The temperature of cavitation, Science (1979) 253 (5026) (1991) 1397–1399.
[30] A. Henglein, Contributions to various aspects of cavitaion chemistry, Adv. Sonochem. 3 (1993) 17–83.
[31] C.M. Sehgal, S.Y. Wang, Threshold intensities and kinetics of sonoreaction of thymine in aqueous solutions at low ultrasonic intensities, J. Am. Chem. Soc. 103 (22) (1981) 6606–6611.
[32] M. Gutierrez, A. Henglein, Chemical action of pulsed ultrasound: observation of an unprecedented intensity effect, J. Phys. Chem. (Easton) 94 (9) (1990) 3625–3628.
[33] A. Henglein, R. Ulrich, J. Lilie, Luminescence and chemical action by pulsed ultrasound, J. Am. Chem. Soc. 111 (6) (1989) 1974–1979.
[34] P. Kanthale, M. Ashokkumar, F. Grieser, Sonoluminescence, sonochemistry (H2O2 yield) and bubble dynamics: frequency and power effects, Ultrason. Sonochem. 15 (2) (2008) 143–150.
[35] C. Petrier, A. Jeunet, J.L. Luche, G. Reverdy, Unexpected frequency effects on the rate of oxidative processes induced by ultrasound, J. Am. Chem. Soc. 114 (8) (1992) 3148–3150.
[36] M. Ashokkumar, et al., Modification of food ingredients by ultrasound to improve functionality: A preliminary study on a model system, Innov. Food Sci. Emerg. Tech. 9 (2) (2008) 155–160.
[37] G. Chatel, L. Novikova, S. Petit, How efficiently combine sonochemistry and clay science? Appl. Clay. Sci. 119 (2016) 193–201.
[38] A. Brotchie, F. Grieser, M. Ashokkumar, Effect of power and frequency on bubble-size distributions in acoustic cavitation, Phys. Rev. Lett. 102 (8) (2009) 084302.
[39] J.D. Seymour, H.C. Wallace, R.B. Gupta, Sonochemical reactions at 640 kHz using an efficient reactor. Oxidation of potassium iodide, Ultrason. Sonochem. 4 (4) (1997) 289–293.
[40] S. Merouani, H. Ferkous, O. Hamdaoui, Y. Rezgui, M. Guemini, A method for predicting the number of active bubbles in sonochemical reactors, Ultrason. Sonochem. 22 (2015) 51–58.
[41] M.J. Bussemaker, D. Zhang, A phenomenological investigation into the opposing effects of fluid flow on sonochemical activity at different frequency and power settings. 1. Overhead stirring, Ultrason. Sonochem. 21 (1) (2014) 436–445.
[42] M. Ashokkumar, M. Ashokkumar, Ultrasonic synthesis of functional materials, Springer, 2016.
[43] R.N. Baig, R.S. Varma, Alternative energy input: mechanochemical, microwave and ultrasound-assisted organic synthesis, Chem. Soc. Rev. 41 (4) (2012) 1559–1584.
[44] K.S. Suslick, et al., Acoustic cavitation and its chemical consequences, Philos. Trans. R. Soc. Lond. Series A Math. Phys. Eng. Sci. 357 (1751) (1999) 335–353.
[45] J. Gao, et al., The investigation of sonocatalytic activity of Er3+: YAlO3/TiO2-ZnO composite in azo dyes degradation, Ultrason. Sonochem. 18 (2) (2011) 541–548.
[46] L.L. He, et al., Synthesis of CaMoO4 microspheres with enhanced sonocatalytic performance for the removal of Acid Orange 7 in the aqueous environment, Sep. Purif. Technol. 276 (2021) 119370.
[47] X.J. Wen, et al., Recent developments on AgI based heterojunction photocatalytic systems in photocatalytic application, Chem. Eng. J. 383 (2020) 123083.
[48] J. Theerthagiri, et al., Application of advanced materials in sonophotocatalytic processes for the remediation of environmental pollutants, J. Hazard. Mater. 412 (2021) 125245.
[49] P. Gholami, A. Khataee, R.D.C. Soltani, A. Bhatnagar, A review on carbon-based materials for heterogeneous sonocatalysis: fundamentals, properties and applications, Ultrason. Sonochem. 58 (2019) 104681.
[50] A. Ziylan, Y. Koltypin, A. Gedanken, N.H. Ince, More on sonolytic and sonocatalytic decomposition of Diclofenac using zero-valent iron, Ultrason. Sonochem. 20 (1) (2013) 580–586.
[51] R. Bhavani, A. Sivasamy, Sonocatalytic degradation of malachite green oxalate by a semiconductor metal oxide nanocatalyst, Ecotoxicol. Environ. Saf. 134 (2016) 403–411.
[52] M. Naderi, S. Asadpour, M. Nekoeinia, M. Kooravand, Ultrasound assisted Sono-Fenton process including FeMnO3 nanocatalysts for degradation of phenazopyridine, J. Mol. Liq. 390 (2023) 122916.
[53] K. Li, S. Wang, C. Chen, Y. Xie, X. Dai, Y. Chen, Sonocatalytic biomaterials, Coord. Chem. Rev. 522 (2025) 216242.
[54] X. Song, L. Yu, L. Chen, Y. Chen, Catalytic biomaterials, Acc. Mater. (Basel) Res. 5 (3) (2024) 271–285.
[55] Z.L. Low, D.Y.S. Low, S.Y. Tang, S. Manickam, K.W. Tan, Z.H. Ban, Ultrasonic cavitation: an effective cleaner and greener intensification technology in the extraction and surface modification of nanocellulose, Ultrason. Sonochem. 90 (2022) 106176.
[56] C. Yao, S. Zhao, L. Liu, Z. Liu, G. Chen, Ultrasonic emulsification: basic characteristics, cavitation, mechanism, devices and application, Front. (Boulder) Chem. Sci. Eng. 16 (11) (2022) 1560–1583.
[57] G. Wang, et al., Design and performance of a novel direct Z-scheme NiGa2O4/CeO2 nanocomposite with enhanced sonocatalytic activity, Sci. Total Environ. 741 (2020) 140192.
[58] L. Zhang, V. Belova, H. Wang, W. Dong, H. Möhwald, Controlled cavitation at nano/microparticle surfaces, Chemistry (Easton) of Materials (Basel) 26 (7) (2014) 2244–2248.
[59] A.J. Melmed, Influence of adsorbed gas on surface diffusion and nucleation, J. Appl. Phys. 37 (1) (1966) 275–279.
[60] V. Belova, D.A. Gorin, D.G. Shchukin, H. Möhwald, Controlled effect of ultrasonic cavitation on hydrophobic/hydrophilic surfaces, ACS Appl. Mater. Interf. 3 (2) (2011) 417–425.
[61] L.O. Hedges, S. Whitelam, Selective nucleation in porous media, Soft. Matter. 9 (41) (2013) 9763–9766.
[62] V. Roldugin, N. Tikhonov, Heterogeneous nucleation on fractal surfaces, Doklady Phys. Chem. (Easton) 383 (2002) 84–87.
[63] A.B. Pandit, P.R. Gogate, S. Mujumdar, Ultrasonic degradation of 2: 4: 6 trichlorophenol in presence of TiO2 catalyst, Ultrason. Sonochem. 8 (3) (2001) 227–231.
[64] J. Wang, B. Guo, X. Zhang, Z. Zhang, J. Han, J. Wu, Sonocatalytic degradation of methyl orange in the presence of TiO2 catalysts and catalytic activity comparison of rutile and anatase, Ultrason. Sonochem. 12 (5) (2005) 331–337.
[65] J.T. Li, M. Li, J.H. Li, H.W. Sun, Decolorization of azo dye direct scarlet 4BS solution using exfoliated graphite under ultrasonic irradiation, Ultrason. Sonochem. 14 (2) (2007) 241–245.
[66] Y. Dai, F. Li, F. Ge, F. Zhu, L. Wu, X. Yang, Mechanism of the enhanced degradation of pentachlorophenol by ultrasound in the presence of elemental iron, J. Hazard. Mater. 137 (3) (2006) 1424–1429.
[67] T. Zhou, Y. Li, F.S. Wong, X. Lu, Enhanced degradation of 2, 4-dichlorophenol by ultrasound in a new Fenton like system (Fe/EDTA) at ambient circumstance, Ultrason. Sonochem. 15 (5) (2008) 782–790.
[68] M.M. Tauber, G.M. Guebitz, A. Rehorek, Degradation of azo dyes by laccase and ultrasound treatment, Appl. Environ. Microbiol. 71 (5) (2005) 2600–2607.
[69] M.A. Ahmed, A.A. Mohamed, Advances in ultrasound-assisted synthesis of photocatalysts and sonophotocatalytic processes: A review, iScience 27 (1) (2024).
[70] S. Hilgenfeldt, S. Grossmann, D. Lohse, A simple explanation of light emission in sonoluminescence, Nature 398 (6726) (1999) 402–405.
[71] T.J. Matula, R.A. Roy, P.D. Mourad, W.B. McNamara III, K.S. Suslick, Comparison of multibubble and single-bubble sonoluminescence spectra, Phys. Rev. Lett. 75 (13) (1995) 2602.
[72] S.J. Putterman, K.R. Weninger, Sonoluminescence: how bubbles turn sound into light, Annu Rev. Fluid. Mech. 32 (1) (2000) 445–476.
[73] R.A. Hiller, S.J. Putterman, K.R. Weninger, Time-resolved spectra of sonoluminescence, Phys. Rev. Lett. 80 (5) (1998) 1090.
[74] K. Matsumoto, T. Makino, T. Ebara, J. Mizuguchi, Characterization of various TiO2 powders used for complete decomposition of organic wastes by means of thermally excited holes at high temperatures, J. Chem. Eng. Jpn. 41 (2) (2008) 51–56.
[75] K. Matsumoto, Y. Sato, T. Ebara, J. Mizuguchi, Hydrogen production from methanol or methane by the use of thermally generated holes in TiO2, J. Chem. Eng. Jpn. 41 (2) (2008) 57–61.

[76] J. Mizuguchi, T. Shinbara, Disposal of used optical disks utilizing thermally-excited holes in titanium dioxide at high temperatures: A complete decomposition of polycarbonate, J. Appl. Phys. 96 (6) (2004) 3514–3519.
[77] H. Shima, H. Takahashi, H. Miyauchi, J. Mizuguchi, Instantaneous and complete decomposition of formaldehyde by thermally activated oxide semiconductors, Materials (Basel) transactions 52 (7) (2011) 1489–1491.
[78] E.V. Skorb, H. Möhwald, D.V. Andreeva, Effect of cavitation bubble collapse on the modification of solids: crystallization aspects, Langmuir. 32 (43) (2016) 11072–11085.
[79] M. Ashokkumar, R. Hall, P. Mulvaney, F. Grieser, Sonoluminescence from aqueous alcohol and surfactant solutions, J. Phys. Chem. (Easton) B 101 (50) (1997) 10845–10850.
[80] E. Cho, J. Choi, Y. Lee, J.M. Park, J. Khim, Sonochemical degradation of reactive black 5 with a composite catalyst of TiO2/single-walled carbon nanotubes, Jpn. J. Appl. Phys. 52 (7S) (2013) 07HE08.
[81] Y.L. Pang, A.Z. Abdullah, Effect of carbon and nitrogen co-doping on characteristics and sonocatalytic activity of TiO2 nanotubes catalyst for degradation of rhodamine B in water, Chem. Eng. J. 214 (2013) 129–138.
[82] P. Liu, T. Zhou, H. Lin, X. Fu, Coupling effect for TiO2/SnO2 compound semiconductor photocatalyst, Acta Physico-Chimica Sinica 17 (3) (2001) 265–269.
[83] J. Zhuang, et al., Photocatalytic degradation of RhB over TiO2 bilayer films: effect of defects and their location, Langmuir 26 (12) (2010) 9686–9694.
[84] J. Zhuang, S. Weng, W. Dai, P. Liu, Q. Liu, Effects of interface defects on charge transfer and photoinduced properties of TiO2 bilayer films, J. Phys. Chem. (Easton) C 116 (48) (2012) 25354–25361.
[85] M. Pirsaheb, N. Moradi, Sonochemical degradation of pesticides in aqueous solution: investigation on the influence of operating parameters and degradation pathway–a systematic review, RSC Adv. 10 (13) (2020) 7396–7423.
[86] S. Chakma, V.S. Moholkar, Investigation in mechanistic issues of sonocatalysis and sonophotocatalysis using pure and doped photocatalysts, Ultrason. Sonochem. 22 (2015) 287–299.
[87] M. Ahmad, E. Ahmed, Z. Hong, W. Ahmed, A. Elhissi, N. Khalid, Photocatalytic, sonocatalytic and sonophotocatalytic degradation of Rhodamine B using ZnO/CNTs composites photocatalysts, Ultrason. Sonochem. 21 (2) (2014) 761–773.
[88] P. Bansal, G.R. Chaudhary, S. Mehta, Comparative study of catalytic activity of ZrO2 nanoparticles for sonocatalytic and photocatalytic degradation of cationic and anionic dyes, Chem. Eng. J. 280 (2015) 475–485.
[89] R.J. Tayade, P.K. Surolia, R.G. Kulkarni, R.V. Jasra, Photocatalytic degradation of dyes and organic contaminants in water using nanocrystalline anatase and rutile TiO2, Sci. Technol. Adv. Mater. 8 (6) (2007) 455.
[90] Q. Sun, Y. Xu, Evaluating intrinsic photocatalytic activities of anatase and rutile TiO2 for organic degradation in water, J. Phys. Chem. (Easton) C 114 (44) (2010) 18911–18918.
[91] M. Andersson, L. Österlund, S. Ljungström, A. Palmqvist, Preparation of nanosize anatase and rutile TiO2 by hydrothermal treatment of microemulsions and their activity for photocatalytic wet oxidation of phenol, J. Phys. Chem. (Easton) B 106 (41) (2002) 10674–10679.
[92] A.L. Linsebigler, G. Lu, J.T. Yates Jr, Photocatalysis on TiO2 surfaces: principles, mechanisms, and selected results, Chem. Rev. 95 (3) (1995) 735–758.
[93] N.S. Allen, N. Mahdjoub, V. Vishnyakov, P.J. Kelly, R.J. Kriek, The effect of crystalline phase (anatase, brookite and rutile) and size on the photocatalytic activity of calcined polymorphic titanium dioxide (TiO2), Polymer (Guildf) Polym. Degrad. Stab. 150 (2018) 31–36.
[94] C.G. Silva, J.L. Faria, Anatase vs. rutile efficiency on the photocatalytic degradation of clofibric acid under near UV to visible irradiation, Photochem. Photobiol. Sci. 8 (5) (2009) 705–711.
[95] J. Zhang, P. Zhou, J. Liu, J. Yu, New understanding of the difference of photocatalytic activity among anatase, rutile and brookite TiO2, Phys. Chem. (Easton) Chem. Phys. (College Park Md) 16 (38) (2014) 20382–20386.
[96] W. Kim, T. Tachikawa, G.h. Moon, T. Majima, W. Choi, Molecular-level understanding of the photocatalytic activity difference between anatase and rutile nanoparticles, Angewandte Chemie 126 (51) (2014) 14260–14265.
[97] K. Zhang, F.J. Zhang, M.L. Chen, W.C. Oh, Comparison of catalytic activities for photocatalytic and sonocatalytic degradation of methylene blue in present of anatase TiO2–CNT catalysts, Ultrason. Sonochem. 18 (3) (2011) 765–772.
[98] M. Chauhan, N. Kaur, P. Bansal, R. Kumar, S. Srinivasan, and G.R. Chaudhary, "Proficient photocatalytic and sonocatalytic degradation of organic pollutants using CuO nanoparticles," , vol. 2020, no. 1, p. 6123178, 2020.
[99] A. Taufik, H. Tju, R. Saleh, Comparison of catalytic activities for sonocatalytic, photocatalytic and sonophotocatalytic degradation of methylene blue in the presence of magnetic Fe3O4/CuO/ZnO nanocomposites, J. Phys. 710 (1) (2016) 012004.
[100] P. Singh, et al., Comparative study of dye degradation using TiO2-activated carbon nanocomposites as catalysts in photocatalytic, sonocatalytic, and photosonocatalytic reactor, Desalination Water Treat. 57 (43) (2016) 20552–20564.
[101] N. Talebian, M.R. Nilforoushan, F.J. Mogaddas, Comparative study on the sonophotocatalytic degradation of hazardous waste, Ceram. Int. 39 (5) (2013) 4913–4921.
[102] J. Abdi, A.J. Sisi, M. Hadipoor, A. Khataee, State of the art on the ultrasonic-assisted removal of environmental pollutants using metal-organic frameworks, J. Hazard. Mater. 424 (2022) 127558.
[103] J. Abdi, M. Vossoughi, N.M. Mahmoodi, I. Alemzadeh, Synthesis of metal-organic framework hybrid nanocomposites based on GO and CNT with high adsorption capacity for dye removal, Chem. Eng. J. 326 (2017) 1145–1158.
[104] M. Oveisi, M.A. Asli, N.M. Mahmoodi, MIL-Ti metal-organic frameworks (MOFs) nanomaterials as superior adsorbents: synthesis and ultrasound-aided dye adsorption from multicomponent wastewater systems, J. Hazard. Mater. 347 (2018) 123–140.
[105] M. Shams, M.H. Dehghani, R. Nabizadeh, A. Mesdaghinia, M. Alimohammadi, A. A. Najafpoor, Adsorption of phosphorus from aqueous solution by cubic zeolitic imidazolate framework-8: modeling, mechanical agitation versus sonication, J. Mol. Liq. 224 (2016) 151–157.
[106] O. Filippou, E.A. Deliyanni, V.F. Samanidou, Fabrication and evaluation of magnetic activated carbon as adsorbent for ultrasonic assisted magnetic solid phase dispersive extraction of bisphenol A from milk prior to high performance liquid chromatographic analysis with ultraviolet detection, J. Chromat. A 1479 (2017) 20–31.
[107] C. Djilani, et al., Adsorption of dyes on activated carbon prepared from apricot stones and commercial activated carbon, J. Taiwan. Inst. Chem. Eng. 53 (2015) 112–121.
[108] J. Komkiene, E. Baltrenaite, Biochar as adsorbent for removal of heavy metal ions [Cadmium (II), Copper (II), Lead (II), Zinc (II)] from aqueous phase, Int. J. Environ. Sci. Tech. (Singap. World Sci.) 13 (2) (2016) 471–482.
[109] F.L. Braghiroli, H. Bouafif, N. Hamza, C.M. Neculita, A. Koubaa, Production, characterization, and potential of activated biochar as adsorbent for phenolic compounds from leachates in a lumber industry site, Environ. Sci. Poll. Res. 25 (26) (2018) 26562–26575.
[110] U. Kumari, S.K. Behera, B. Meikap, A novel acid modified alumina adsorbent with enhanced defluoridation property: kinetics, isotherm study and applicability on industrial wastewater, J. Hazard. Mater. 365 (2019) 868–882.
[111] M. Alnajjar, A. Hethnawi, G. Nafie, A. Hassan, G. Vitale, N.N. Nassar, Silica-alumina composite as an effective adsorbent for the removal of metformin from water, J. Environ. Chem. Eng. 7 (3) (2019) 102994.
[112] E. Zanin, et al., Adsorption of heavy metals from wastewater graphic industry using clinoptilolite zeolite as adsorbent, Process Safe. Environ. Protect. 105 (2017) 194–200.
[113] T.H. Pham, B.K. Lee, J. Kim, Improved adsorption properties of a nano zeolite adsorbent toward toxic nitrophenols, Process Safe. Environ. Protect. 104 (2016) 314–322.
[114] I. Ihsanullah, Applications of MOFs as adsorbents in water purification: progress, challenges and outlook, Curr. Opin. Environ. Sci. Health N. Hav. 26 (2022) 100335.
[115] M. Safari, A. Khataee, R.D.C. Soltani, R. Rezaee, Ultrasonically facilitated adsorption of an azo dye onto nanostructures obtained from cellulosic wastes of broom and cooler straw, J. Colloid. Interface Sci. 522 (2018) 228–241.
[116] A.J. Sisi, A. Khataee, M. Fathinia, B. Vahid, Y. Orooji, Comparative study of sonocatalytic process using MOF-5 and peroxydisulfate by central composite design and artificial neural network, J. Mol. Liq. 316 (2020) 113801.
[117] A.J. Sisi, M. Fathinia, A. Khataee, Y. Orooji, Systematic activation of potassium peroxydisulfate with ZIF-8 via sono-assisted catalytic process: mechanism and ecotoxicological analysis, J. Mol. Liq. 308 (2020) 113018.
[118] S. Chakma, V.S. Moholkar, Physical mechanism of sono-fenton process, AIChE J. 59 (11) (2013) 4303–4313.
[119] Y.S. Ma, Short review: current trends and future challenges in the application of sono-Fenton oxidation for wastewater treatment, Sustain. Environ. Res. 22 (5) (2012) 271–278.
[120] K.S. Hong, H. Xu, H. Konishi, X. Li, Direct water splitting through vibrating piezoelectric microfibers in water, J. Phys. Chem. Lett. 1 (6) (2010) 997–1002.
[121] K. Kubota, Y. Pang, A. Miura, H. Ito, Redox reactions of small organic molecules using ball milling and piezoelectric materials, Science (1979) 366 (6472) (2019) 1500–1504.
[122] K. Wang, D. Shao, L. Zhang, Y. Zhou, H. Wang, W. Wang, Efficient piezo-catalytic hydrogen peroxide production from water and oxygen over graphitic carbon nitride, J. Mater. (Basel) Chem. (Easton) A 7 (35) (2019) 20383–20389.
[123] Y. Wang, et al., Ultrasonic activation of inert poly (tetrafluoroethylene) enables piezocatalytic generation of reactive oxygen species, Nat. Commun. 12 (1) (2021) 3508.
[124] J. Lipkowski and P.N. Ross, "Electrocatalysis," 1998.
[125] S. Li, et al., Few-layer transition metal dichalcogenides (MoS2, WS2, and WSe2) for water splitting and degradation of organic pollutants: understanding the piezocatalytic effect, Nano Energy 66 (2019) 104083.
[126] R. Su, et al., Strain-engineered nano-ferroelectrics for high-efficiency piezocatalytic overall water splitting, Angew. Chem. Int. Edn. 60 (29) (2021) 16019–16026.
[127] I.S. Vatlin, et al., Bacteriostatic effect of piezoelectric poly-3-hydroxybutyrate and polyvinylidene fluoride polymer films under ultrasound treatment, Polymers (Basel) 12 (1) (2020) 240.
[128] B. Bagchi, N.A. Hoque, N. Janowicz, S. Das, M.K. Tiwari, Re-usable self-poled piezoelectric/piezocatalytic films with exceptional energy harvesting and water remediation capability, Nano Energy 78 (2020) 105339.
[129] T.D. Raju, S. Veeralingam, S. Badhulika, Polyvinylidene fluoride/ZnSnO3 nanocube/Co3O4 nanoparticle thermoplastic composites for ultrasound-assisted piezo-catalytic dye degradation, ACS Appl. Nano Mater. (Basel) 3 (5) (2020) 4777–4787.
[130] F. Li, et al., Ultrahigh piezoelectricity in ferroelectric ceramics by design, Nat. Mater. 17 (4) (2018) 349–354.
[131] M.B. Starr, X. Wang, Coupling of piezoelectric effect with electrochemical processes, Nano Energy 14 (2015) 296–311.

[132] C. Hu, et al., Exceptional cocatalyst-free photo-enhanced piezocatalytic hydrogen evolution of carbon nitride nanosheets from strong in-plane polarization, Adv. Mater. (Basel) 33 (24) (2021) 2101751.
[133] Y. Hu, et al., Lattice distortion induced internal electric field in TiO2 photoelectrode for efficient charge separation and transfer, Nat. Commun. 11 (1) (2020) 2129.
[134] J. Shi, M.B. Starr, X. Wang, Band structure engineering at heterojunction interfaces via the piezotronic effect, Adv. Mater. (Basel) 24 (34) (2012) 4683–4691.
[135] M.B. Starr, J. Shi, X. Wang, Piezopotential-driven redox reactions at the surface of piezoelectric materials, Angew. Chem. Int. Edn. 51 (24) (2012) 5962–5966.
[136] Y. Zhang, et al., Polarisation tuneable piezo-catalytic activity of Nb-doped PZT with low Curie temperature for efficient CO 2 reduction and H 2 generation, Nanoscale Adv. 3 (5) (2021) 1362–1374.
[137] V. Bystrov, et al., Piezoelectric nanomaterials for biomedical applications, in: Berlin: Springer) Piezoelectricity and ferroelectricity in biomaterials: from proteins to self-assembled peptide nanotubes 7, 2012, pp. 187–211.
[138] M. Durruthy-Rodríguez, J. Costa-Marrero, M. Hernández-García, F. Calderón-Piñar, J. Yañez-Limón, Photoluminescence in "hard" and "soft" ferroelectric ceramics, Appl. Phys. (College Park Md) A 98 (3) (2010) 543–550.
[139] R. Bhatnagar, V. Yadav, U. Kumar, M.F. Carrasco, Piezoelectric energy harvesting: from fundamentals to advanced applications, Energ. Tech. (Singap. World Sci.) 13 (4) (2025) 2401455.
[140] F. Bößl, et al., Importance of energy band theory and screening charge effect in piezo-electrocatalytical processes, Electrochim. Acta 462 (2023) 142730.
[141] S. Vasilev, P. Zelenovskiy, D. Vasileva, A. Nuraeva, V.Y. Shur, A.L. Kholkin, Piezoelectric properties of diphenylalanine microtubes prepared from the solution, J. Phys. (College Park Md) Chem. (Easton) Solids 93 (2016) 68–72.
[142] T. Someya, Stretchable electronics, John Wiley & Sons, 2013.
[143] J. Wang, et al., Piezoelectric nanocellulose thin film with large-scale vertical crystal alignment, ACS Appl. Mater. Interf. 12 (23) (2020) 26399–26404.
[144] E. Praveen, S. Murugan, K. Jayakumar, Investigations on the existence of piezoelectric property of a bio-polymer–chitosan and its application in vibration sensors, RSC Adv. 7 (56) (2017) 35490–35495.
[145] I. Guy, S. Muensit, E. Goldys, Extensional piezoelectric coefficients of gallium nitride and aluminum nitride, Appl. Phys. Lett. 75 (26) (1999) 4133–4135.
[146] F. Yang, et al., Wafer-scale heterostructured piezoelectric bio-organic thin films, Science (1979) 373 (6552) (2021) 337–342.
[147] R.E. Newnham, Properties of materials: anisotropy, symmetry, structure, OUP, Oxford, 2004.
[148] R. Su, et al., Engineering heterostructured Ti 4 O 5/BaTiO 3 ferroelectric by surface reconstruction for enhanced photocatalytic CO 2 reduction, Inorg. Chem. Front. 10 (13) (2023) 3947–3954.
[149] Z. Zhao, et al., Exclusive enhancement of catalytic activity in Bi 0.5 Na 0.5 TiO 3 nanostructures: new insights into the design of efficient piezocatalysts and piezo-photocatalysts, J. Mater. (Basel) Chem. (Easton) A 8 (32) (2020) 16238–16245.
[150] W. Wang, L. Zhou, S. Hu, K.S. Novoselov, Y. Cao, Visualizing piezoelectricity on 2D crystals nanobubbles, Adv. Funct. Mater. 31 (6) (2021) 2005053.
[151] S.V. Kalinin, D.A. Bonnell, Screening phenomena on oxide surfaces and its implications for local electrostatic and transport measurements, Nano Lett. 4 (4) (2004) 555–560.
[152] Y. Wang, et al., Piezo-catalysis for nondestructive tooth whitening, Nat. Commun. 11 (1) (2020) 1328.
[153] F. Bößl, I. Tudela, Piezocatalysis: can catalysts really dance? Curr. Opin. Green Sustain. Chem. (Easton) 32 (2021) 100537.
[154] W. Qian, W. Yang, Y. Zhang, C.R. Bowen, Y. Yang, Piezoelectric materials for controlling electro-chemical processes, Nanomicro Lett. 12 (1) (2020) 149.
[155] X. Zhou, B. Shen, J. Zhai, N. Hedin, Reactive oxygenated species generated on iodide-doped BiVO4/BaTiO3 heterostructures with Ag/Cu nanoparticles by coupled piezophototronic effect and plasmonic excitation, Adv. Funct. Mater. 31 (13) (2021) 2009594.
[156] A. Zhang, et al., Vibration catalysis of eco-friendly Na0. 5K0. 5NbO3-based piezoelectric: an efficient phase boundary catalyst, Appl. Catal. B Environ. 279 (2020) 119353.
[157] X. Liu, L. Xiao, Y. Zhang, H. Sun, Significantly enhanced piezo-photocatalytic capability in BaTiO3 nanowires for degrading organic dye, J. Materiom. 6 (2) (2020) 256–262.
[158] M. Shah et al., "Synergistic effects in triboelectric charge-driven redox reactions," Available at SSRN 5338070.
[159] T. Gan, et al., Unveiling Janus chemical processes in contact-electro-chemistry through oxygen reduction reactions, J. Am. Chem. Soc. (2025).
[160] C. Porwal, et al., Effect of surface/bulk polarization on piezocatalysis using BaTiO3, J. Mater. (Basel) Sci. 35 (8) (2024) 573.
[161] H. Sudrajat, H.Y. Hsu, F. Jérôme, J.C. Colmenares, Mechanoredox-catalyzed organic synthesis with piezoelectric materials: Quo Vadis? ChemCatChem 17 (6) (2025) e202401814.
[162] Y. He, et al., Piezocatalyzed decarboxylative acylation of quinoxalin-2 (1 H)-ones using ball milling, ACS Sustain. Chem. Eng. 11 (3) (2023) 910–920.
[163] Y. Pang, J.W. Lee, K. Kubota, H. Ito, Solid-state radical C– H trifluoromethylation reactions using ball milling and piezoelectric materials, Angew. Chem. Int. Edn. 59 (50) (2020) 22570–22576.
[164] Z. Wang, et al., Temporal control in mechanically controlled atom transfer radical polymerization using low ppm of Cu catalyst, ACS Macro Lett. 6 (5) (2017) 546–549.
[165] Q. He, J. Briscoe, Piezoelectric energy harvester technologies: synthesis, mechanisms, and multifunctional applications, ACS Appl. Mater. Interf. 16 (23) (2024) 29491–29520.
[166] X. Du, et al., Emerging piezocatalysts: metal–organic frameworks and their derivatives, Nano Today 65 (2025) 102841.
[167] L. Du, et al., Insights on the mechanism of piezocatalysis: switchable screen charge effects enhanced the piezo-photocatalytic activities of BaTiO3 ferroelectric platelets, J. Alloy. Compd. 1021 (2025) 179669.
[168] Z. Chen, H. Zhou, F. Kong, M. Wang, Piezocatalytic oxidation of 5-hydroxymethylfurfural to 5-formyl-2-furancarboxylic acid over Pt decorated hydroxyapatite, Appl. Catal. B Environ. 309 (2022) 121281.
[169] Y. Miao, et al., Oxygen vacancy-induced hydroxyl dipole reorientation in hydroxyapatite for enhanced piezocatalytic activity, Nano Energy 100 (2022) 107473.
[170] V. Tiron, et al., Piezo-ferroelectric response of bismuth ferrite based thin films and their related photo/piezocatalytic performance, Ceram. Int. 49 (12) (2023) 20304–20314.
[171] H. Zhou, J. Cao, Y. Ji, M. Xia, W. Yao, Twin boundaries-induced centrosymmetric breaking of hollow CaTiO3 nanocuboids for piezocatalytic hydrogen evolution, Small 20 (44) (2024) 2402679.
[172] Y. Ji, M. Xia, H. Wang, W. Yao, Defect-driven piezocatalysis in zinc hydroxystannate: role of oxygen vacancies and interfaces, Mater. (Basel) Today Commun. 44 (2025) 112046.
[173] X. Liao, H. Xie, B. Liao, S. Hou, Y. Yu, X. Fan, Ball milling induced strong polarization electric fields in Cu3B2O6 crystals for high efficiency piezocatalysis, Nano Energy 94 (2022) 106890.
[174] Y. Yao, et al., Piezoelectric BaTiO3 with the milling treatment for highly efficient piezocatalysis under vibration, J. Alloy. Compd. 905 (2022) 164234.
[175] Z. Kang, E. Lin, N. Qin, J. Wu, B. Yuan, D. Bao, Effect of oxygen vacancies and crystal symmetry on piezocatalytic properties of Bi 2 WO 6 ferroelectric nanosheets for wastewater decontamination, Environ. Sci. Nano 8 (5) (2021) 1376–1388.
[176] H. Djani, E. Bousquet, A. Kellou, P. Ghosez, First-principles study of the ferroelectric Aurivillius phase Bi 2 WO 6, Phys. Rev. B—Condens. Matter Mater. (Basel) Phys. (College Park Md) 86 (5) (2012) 054107.
[177] H.M. Elmehdi, et al., Diode characteristics, piezo-photocatalytic antibiotic degradation and hydrogen production of Ce3+ doped ZnO nanostructures, Chemosphere 350 (2024) 141015.
[178] C. Liu, et al., Improvement in the piezoelectric performance of a ZnO nanogenerator by a combination of chemical doping and interfacial modification, J. Phys. Chem. (Easton) C 120 (13) (2016) 6971–6977.
[179] M. Laurenti, N. Garino, G. Canavese, S. Hernandez, V. Cauda, Piezo-and photocatalytic activity of ferroelectric ZnO: Sb thin films for the efficient degradation of rhodamine-β dye pollutant, ACS Appl. Mater. Interf. 12 (23) (2020) 25798–25808.
[180] J. Dai, et al., Enhanced piezocatalytic activity of Sr0. 5Ba0. 5Nb2O6 nanostructures by engineering surface oxygen vacancies and self-generated heterojunctions, ACS Appl. Mater. Interf. 13 (6) (2021) 7259–7267.
[181] P. Wang, et al., Impact of oxygen vacancy occupancy on piezo-catalytic activity of BaTiO3 nanobelt, Appl. Catal. B Environ. 279 (2020) 119340.
[182] Z. Wang, et al., A contact-electro-catalysis process for producing reactive oxygen species by ball milling of triboelectric materials, Nat. Commun. 15 (1) (2024) 757.
[183] C. Xu, S. Li, Y. Zhang, Z. Wang, Z.L. Wang, D. Wei, Contact-electro-chemistry induced by flow electrification in dielectric tubes, Nano Energy 134 (2025) 110526.
[184] Z.L. Wang, A.C. Wang, On the origin of contact-electrification, Materials (Basel) Today 30 (2019) 34–51.
[185] Z.L. Wang, Contact-Electrification of Matter, Springer Nature, 2025.
[186] J. Lowell, A. Rose-Innes, Contact electrification, Adv. Phys. 29 (6) (1980) 947–1023.
[187] S. Lin, X. Chen, Z.L. Wang, Contact electrification at the liquid–solid interface, Chem. Rev. 122 (5) (2021) 5209–5232.
[188] C.K. Ao, et al., Balancing charge dissipation and generation: mechanisms and strategies for achieving steady-state charge of contact electrification at interfaces of matter, J. Mater. (Basel) Chem. (Easton) A 10 (37) (2022) 19572–19605.
[189] Z. Chen, et al., Recent progress of solid–liquid interface-mediated contact-electro-catalysis, Langmuir 40 (11) (2024) 5557–5570.
[190] M.N. Liu, et al., Strategies for improving contact-electro-catalytic efficiency: A review, Nanomaterials 15 (5) (2025) 386.
[191] X. Li, W. Tong, Contact-electro-catalysis under natural and industrial conditions: mechanisms, strategies, and challenges, J. Mater. (Basel) Chem. (Easton) A 12 (31) (2024) 19783–19805.
[192] Z. Liang, W. Li, J. Tu, F.R. Fan, Mechanically induced contact-electro-catalysis: free radical generation, reaction pathways, and catalytic applications, ChemCatChem 17 (11) (2025) e202500282.
[193] X. Huo, S. Li, B. Sun, Z.L. Wang, D. Wei, Recent progress of chemical reactions induced by contact electrification, Molecules 30 (3) (2025) 584.
[194] X. Dong, Z. Wang, Y. Hou, T. Wang, F.J. Lv, W. Tang, Quantified analysis on the conversion from contact electrification to contact-electro-catalysis and the performance of contact-electro-catalysts, J. Catal. (2025) 116153.
[195] S. Li, et al., Contributions of different functional groups to contact electrification of polymers, Adv. Mater. (Basel) 32 (25) (2020) 2001307.
[196] J. Zhang, S. Lin, Z.L. Wang, Triboelectric nanogenerator array as a probe for in situ dynamic mapping of interface charge transfer at a liquid–solid contacting, ACS Nano 17 (2) (2023) 1646–1652.

[197] J. Nie, et al., Probing contact-electrification-induced electron and ion transfers at a liquid–solid interface, Adv. Mater. (Basel) 32 (2) (2020) 1905696.
[198] F. Zhan, et al., Electron transfer as a liquid droplet contacting a polymer surface, ACS Nano 14 (12) (2020) 17565–17573.
[199] M. Sun, Q. Lu, Z.L. Wang, B. Huang, Understanding contact electrification at liquid–solid interfaces from surface electronic structure, Nat. Commun. 12 (1) (2021) 1752.
[200] S. Lin, L. Zhu, Z. Tang, Z.L. Wang, Spin-selected electron transfer in liquid–solid contact electrification, Nat. Commun. 13 (1) (2022) 5230.
[201] J. Zhang, S. Lin, Z.L. Wang, Electrostatic charges regulate chemiluminescence by electron transfer at the liquid–solid interface, J. Phys. Chem. (Easton) B 126 (14) (2022) 2754–2760.
[202] C. Xu, S. Li, Z. Yang, M. Willatzen, Z.L. Wang, D. Wei, Contact-electro-luminescence triggered by triboelectric charge, Chem. Eng. J. 501 (2024) 157754.
[203] S. Lin, L. Xu, A.Chi Wang, Z.L. Wang, Quantifying electron-transfer in liquid-solid contact electrification and the formation of electric double-layer, Nat. Commun. 11 (1) (2020) 399.
[204] Y. Wei, X. Li, Z. Yang, J. Shao, Z.L. Wang, D. Wei, Contact electrification at the solid–liquid transition interface, Materials (Basel) Today 74 (2024) 2–11.
[205] X. Li, Z.L. Wang, D. Wei, Nanogenerators via dynamic regulation of electrical double layer, Nano Trends (2024) 100062.
[206] Z. Wang, X. Dong, F.J. Lv, W. Tang, A perspective on contact-electro-catalysis based on frontier molecular orbitals, Mater. (Basel) Adv. 5 (16) (2024) 6373–6377.
[207] H. Zou, et al., Quantifying the triboelectric series, Nat. Commun. 10 (1) (2019) 1427.
[208] S. Lin, M. Zheng, J. Luo, Z.L. Wang, Effects of surface functional groups on electron transfer at liquid–solid interfacial contact electrification, ACS Nano 14 (8) (2020) 10733–10741.
[209] J. Ma, F. Wang, M. Mostafavi, Ultrafast chemistry of water radical cation, H2O•+, in aqueous solutions, Molecules 23 (2) (2018) 244.
[210] Z.H. Loh, et al., Observation of the fastest chemical processes in the radiolysis of water, Science (1979) 367 (6474) (2020) 179–182.
[211] Y. Gauduel, S. Pommeret, A. Migus, A. Antonetti, Some evidence of ultrafast H2O +-water molecule reaction in femtosecond photoionization of pure liquid water: influence on geminate pair recombination dynamics, Chem. Phys. 149 (1-2) (1990) 1–10.
[212] A. Berbille, et al., Mechanism for generating H2O2 at water-solid interface by contact-electrification, Adv. Mater. (Basel) 35 (46) (2023) 2304387.
[213] Y. Zhao, et al., The process of free radical generation in contact electrification at solid-liquid interface, Nano Energy 112 (2023) 108464.
[214] J. Zhao, X. Zhang, J. Xu, W. Tang, Z.Lin Wang, F. Ru Fan, Contact-electro-catalysis for direct synthesis of H2O2 under ambient conditions, Angew. Chem. Int. Edn. 62 (21) (2023) e202300604.
[215] J. Liu, et al., Nonaqueous contact-electro-chemistry via triboelectric charge, J. Am. Chem. Soc. 146 (46) (2024) 31574–31584.
[216] F. Galembeck, T.A. Burgo, L.B. Balestrin, R.F. Gouveia, C.A. Silva, A. Galembeck, Friction, tribochemistry and triboelectricity: recent progress and perspectives, RSC Adv. 4 (109) (2014) 64280–64298.
[217] L.P. Santos, et al., Water reactivity in electrified interfaces: the simultaneous production of electricity, hydrogen, and hydrogen peroxide at room temperature, Langmuir 39 (16) (2023) 5840–5850.
[218] S. Shaik, R. Ramanan, D. Danovich, D. Mandal, Structure and reactivity/selectivity control by oriented-external electric fields, Chem. Soc. Rev. 47 (14) (2018) 5125–5145.
[219] X. Du, et al., Modulating electronic structures of inorganic nanomaterials for efficient electrocatalytic water splitting, Angew. Chem. Int. Edn. 58 (14) (2019) 4484–4502.
[220] X. Song, et al., One-step formation of urea from carbon dioxide and nitrogen using water microdroplets, J. Am. Chem. Soc. 145 (47) (2023) 25910–25916.
[221] X. Song, Y. Meng, R.N. Zare, Spraying water microdroplets containing 1, 2, 3-triazole converts carbon dioxide into formic acid, J. Am. Chem. Soc. 144 (37) (2022) 16744–16748.
[222] M.A. Mehrgardi, M. Mofidfar, R.N. Zare, Sprayed water microdroplets are able to generate hydrogen peroxide spontaneously, J. Am. Chem. Soc. 144 (17) (2022) 7606–7609.
[223] S. Li, Z. Zhang, P. Peng, X. Li, Z.L. Wang, D. Wei, A green approach to induce and steer chemical reactions using inert solid dielectrics, Nano Energy 122 (2024) 109286.
[224] X. Huo, S. Li, B. Sun, Z. Wang, D. Wei, Revealing the role of interfacial charge transfer in mechanoluminescence, Nanomaterials 15 (9) (2025) 656.
[225] K. Lee, S. Bose, X. Song, S.Q. Choi, R.N. Zare, Continuous flow contact electrocatalysis for hydrogen peroxide production, J. Phys. Chem. (Easton) C 129 (13) (2025) 6254–6261.
[226] Y. Su, A. Berbille, Z.L. Wang, W. Tang, Water-solid contact electrification and catalysis adjusted by surface functional groups, Nano Res. 17 (4) (2024) 3344–3351.
[227] Y. Chai, W. Dai, G. Wu, N. Guan, L. Li, Confinement in a zeolite and zeolite catalysis, Acc. Chem. Res. 54 (13) (2021) 2894–2904.
[228] Y. Zhang, et al., Advances in metastable phase catalysis with thermodynamic-kinetic adaptability, Materials (Basel) Today (2025).
[229] J. Liu, et al., Modular contact-electro-chemistry based on dielectrics with work function-tunable metal coatings, Nano Energy (2025) 111389.
[230] M. Shah, et al., Synergistic effects in triboelectric charge-driven redox reactions, Nano Energy (2025) 111380.
[231] Y. Nan, J. Shao, M. Willatzen, Z.L. Wang, Understanding contact electrification at water/polymer interface, Research (2022).